# Final: Enhancing Regenerative Braking Systems in Electric Vehicles

Group Members: Omar Jaber and Shayne Martin

Paper Results Duplication

**Abstract:**

This project focuses on the design and analysis of a control-oriented regenerative braking framework for electric vehicles (EVs) that use a brushless DC (BLDC) motor as both the traction and generating machine. Regenerative braking systems (RBS) recover kinetic energy during deceleration and convert it into electrical energy stored in the battery, improving overall efficiency and driving range. However, practical challenges arise when trying to maintain vehicle stability, achieve a natural brake-pedal feel, and respect converter and battery limitations, especially under low-friction road conditions and at a high state of charge.

In this report, we develop a mathematical model of the vehicle's longitudinal dynamics, aerodynamic drag, rolling resistance, and gravitational effects, and pair it with a BLDC motor model operating in regenerative mode. The BLDC windings and inverter are reconfigured to function as a boost converter, allowing back EMF to be stepped up to the DC link voltage even at low speeds. MATLAB models are then used to simulate braking scenarios over different initial speeds and deceleration levels, estimate the fraction of kinetic energy that can be routed back to the battery, and examine how converter duty cycle, battery resistance, and current limits constrain this recovery. The framework provides a structured path toward controller design that blends friction and regenerative braking while preserving stability and driver comfort.

# Introduction

## Motivation

Electric vehicles are central to the transition toward sustainable transportation because they can dramatically reduce greenhouse-gas emissions and primary energy consumption compared with internal-combustion engine vehicles. While advances in battery technology and motor efficiency are important, braking strategy also plays a key role in the real-world range of an EV. Every time the driver slows down, the vehicle either:

- Dissipates kinetic energy as heat in friction brakes, or
- Recovers a portion of that energy through regenerative braking and sends it back to the battery or DC link.

The more effectively this kinetic energy is recovered during everyday driving (stop-and-go traffic, moderate decelerations, highway exits), the more the EV's effective driving range and brake-system life can be improved.

## Existing Work

Recent studies have proposed BLDC-based regenerative braking frameworks, wheel-slip control strategies for in-wheel motors, and comprehensive reviews of regenerative braking architectures and control methods. These works collectively show that:

- BLDC machines are attractive for traction and regeneration due to high efficiency, wide speed range, and good torque density.

- Slip-ratio and wheel-slip controllers are necessary to avoid wheel lock and maintain stability, especially on low-adhesion surfaces.

### Limitations of Existing Work

In this project, we propose a control framework that combines:

- A BLDC motor model operating in regenerative (generator) mode.
- A boost-converter representation of the inverter/battery interface using volt-second and charge-balance equations.
- A braking strategy that maps driver pedal input into regenerative current commands and friction-brake torque while respecting stability and electrical limits.

## Our approach

In this project, we propose a control framework that combines:

- A BLDC motor model operating in regenerative mode
- A slip ratio-based stability controller implemented in MATLAB
- A  brake pedal to the current mapping that defines regenerative braking torque

### Contributions

The main contributions of this work are:

- A mathematical model of EV longitudinal dynamics with explicit aerodynamic, rolling, and gravitational forces.
- A BLDC regenerative model that shows how duty cycle, armature current, and battery resistance limit the achievable boost ratio and charging voltage.
- A control-oriented mapping from brake-pedal command to regenerative current, with space to include fuzzy logic and slip-ratio control in future work.
- MATLAB simulations and analytic results that illustrate how initial speed, desired deceleration, and electrical constraints jointly determine the recoverable energy fraction.

## Problem Statement

The main challenge in electric vehicles (EVs) is to design a regenerative braking control system that recovers as much kinetic energy as possible during deceleration while still providing safe, stable, and comfortable braking for the driver. This control system must operate reliably over a wide range of speeds, road slopes, and driving conditions, and it must respect practical limitations of the battery and any auxiliary energy storage (such as maximum charging power, state-of-charge limits, and thermal constraints).

In an EV, the BLDC motor, power converter, and mechanical brakes are tightly coupled. During braking, the BLDC motor must switch from motoring to generating mode, the converter duty cycle must be adjusted to regulate DC-link voltage and current, and the mechanical friction brakes must be blended with regenerative torque to maintain proper front–rear brake force distribution and vehicle stability. In practice, this is complicated by nonlinear vehicle dynamics, changes in tire–road conditions, and the limited ability of the battery to accept high charging currents, especially at low temperatures or high state of charge.

Therefore, the core problem addressed in this project is to develop and analyze a regenerative braking control framework that:

- Translates the driver's brake pedal input into coordinated commands for BLDC generator torque, converter duty cycle, and friction braking.
- Maximizes electrical energy delivered back to the DC link and storage system without violating battery or converter constraints.
- Maintains consistent braking feel and vehicle stability across different driving scenarios and road grades.

This problem will be studied using system-level models of the vehicle, BLDC motor in generator mode, and power electronics, implemented and evaluated in MATLAB/Simulink.

## BLDC Dynamics Model

The following figure shows a simple sketch of the Brushless DC (BLDC) motor used in EVs and will be used as a crucial component for our project. This will function as the main driving component as well as the device that will collect the energy in the regenerative braking mode. The BLDC motor functions as permanent magnets are fixed on the rotor, while armature windings are fixed to the stator with a laminated steel core. As the rotor in the BLDC rotates, it creates a magnetic field that can be used to collect energy while seamlessly providing a brake force due to the fact that a battery can be considered as a load during the regenerative mode.

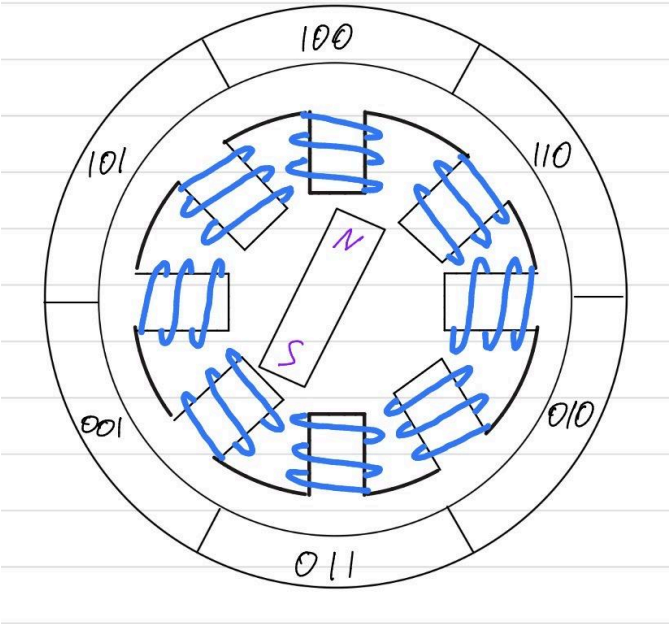


**Fig 1: Brushless DC Motor Sketch.**

The BLDC motor is a great solution to restoring energy to the supply battery; however, it can be complex to control, as many factors must be considered for proper operation. Firstly, we need to

be able to know the rotor's position at all times to properly sustain the motion of the windings. This can be achieved by using either Hall effect sensors or coil EMF measurements.

## BLDC Motor Control

The BLDC motor control is a crucial part of the electronic inverter system, in which communication is established with the BLDC motor control through the order of conduction on the inverter bridge arm. This is typically done by using an H-bridge inverter circuit, shown in the figure below.

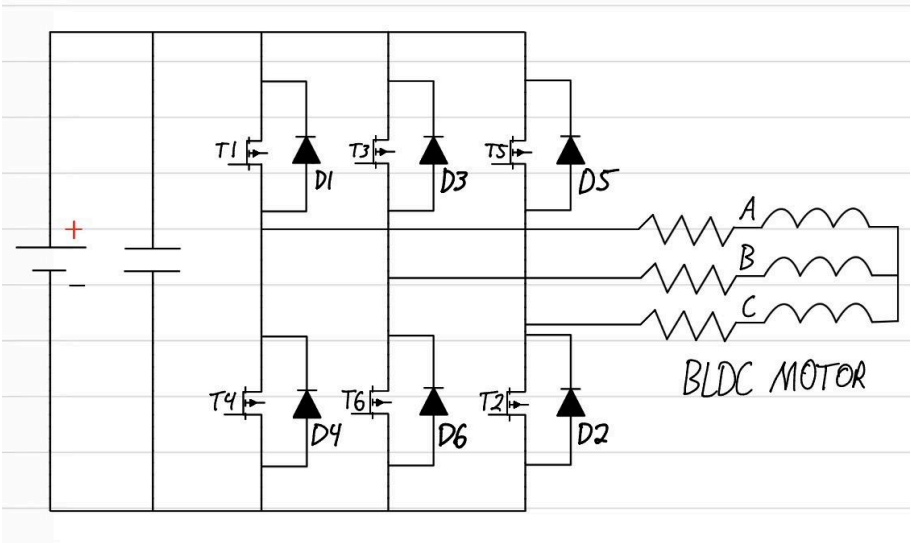


**Fig 2: H-Bridge Inverter Circuit.**

This is considered the basic drive circuit for the BLDC motor, which is powered by a DC power supply to provide the energy to power the motor. The circuit shows that each motor lead is connected to high-side and low-side switches.

In order to control the BLDC motor, we will need to determine the rotor position using Hall effect sensors, which can be created by dividing the BLDC voltage into six sectors, which can be shown in the figure below.

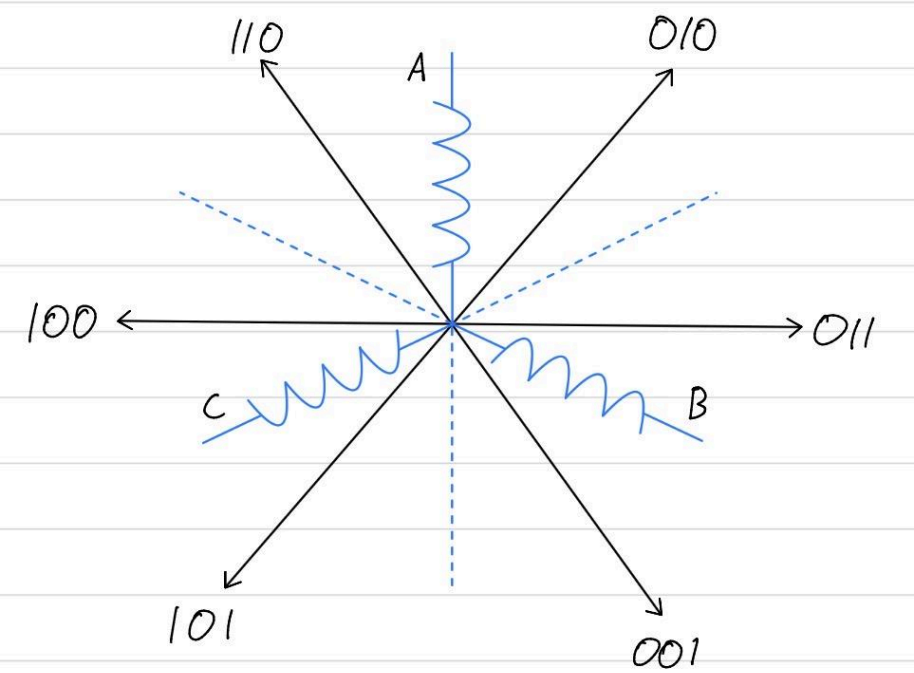


**Fig 3: BLDC motor six-sector voltage vector.**

This can yield sufficient results, as the BLDC motor is divided into six sectors, and the Hall signal has six states, providing a one-to-one correspondence. A crucial component to consider is the fact that the BLDC motor behaves as a generator under braking; therefore, it will create a back EMF, which is the voltage generated while the motor is running, opposing the voltage being applied to it. This is created by the motor's rotation as the coils create a magnetic field, which is directly proportional to the motor's speed. A simple representation of the Hall signal vs the back EMF produced based on the angle of rotation can be shown below

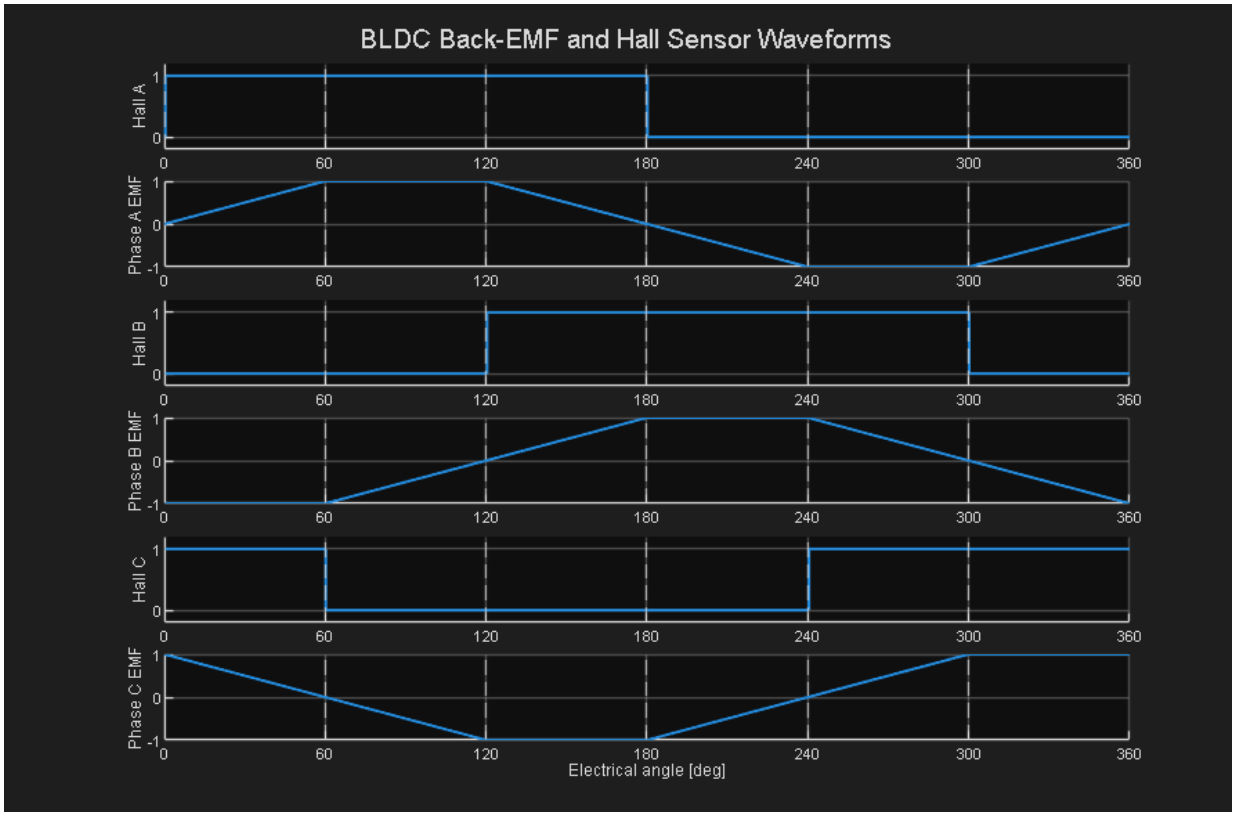


**Fig 4: Hall Sensor vs. Back EMF Waveforms.**

We can collect the energy produced by the back EMF to supply voltage to the battery; however, at low speeds, this EMF is not sufficient to charge the battery directly. To compensate for this, we can use the BLDC's own phase inductances within the motor windings and represent them as a boost converter by reconfiguring the MOSFET device (which is a common device for high-power applications due to its low impedance) by turning off all high-side MOSFETs and using PWM (Pulsewidth Modulation) to control the low-side MOSFETs within the H-bridge inverter circuit.

The fundamental equation to represent the inductor balance during PWM can be derived from the principle of the volt-second balance shown below.

$$\int_{t}^{t+T_S} v_L dt = 0$$

Where $v_L$ is the equivalent inductor voltage over one electric cycle

And the final form giving

$$\int_{t}^{t+T_S} v_L dt = DT_s\left[2V_{emf} - i_a(2R)\right] + D'T_s\left[2V_{emf} - i_a(2R) - V_{dc}\right] = 0; \quad (1)$$

Solving for armature current $i_a$

$$i_a = \frac{2V_{emf}}{D'2R_b+2R} \quad (2)$$

Where $T_s$ is the switching period, $V_{emf}$ is the back EMF, $D$ is the duty cycle of the MOSFET ON and $D' = 1 - D$ the MOSFET OFF.

This equation shows that the current will grow when the duty cycle $D'$ decreases and the battery resistance $R_b$ will affect the armature current significantly.

Similarly to the volt-second balance equation, the battery current or charge balance over the switching period using the principle of the capacitor charge balance equation yields.

$$\int_{t}^{t+T_s} id_c dt = DT_s\left(-\frac{V_{dc}}{R_b}\right) + D'T_s\left(i_a - \frac{V_{dc}}{R_b}\right) \quad (3)$$

Now, substituting our armature current equation with the capacitor charge balance equation gives.

$$T(D') = \frac{V_{dc}}{V_{emf}} = \frac{2}{D'+2\frac{K}{D'}} \text{ where } K = \frac{R}{R_b} \quad (4)$$

$R$ is the internal resistance

This equation describes how much the boost stage increases the voltage.

We can evaluate the maximum conversion ratio by differentiating equation (4) with respect to $D'$

$$\frac{dT}{dD'} = 2 \bullet \frac{\left(2K-D'^2\right)}{\left(D^2+2K\right)^2} \quad (5)$$

Setting the derivative to zero obtains

$$D = \sqrt{2K}$$

Plugging this into equation (4) gives

$$\frac{1}{\sqrt{2K}}$$

This means that when the battery resistance is high, the maximum boost ratio is small, and when $K > 0.5$ the conversion ratio becomes less than 1, meaning there will be no regeneration as $V_{dc} < V_{emf}$. In other words, the dynamic energy of the EV will be lost to braking torque and heat rather than being recovered into the battery. A simple plot of this process is shown below.

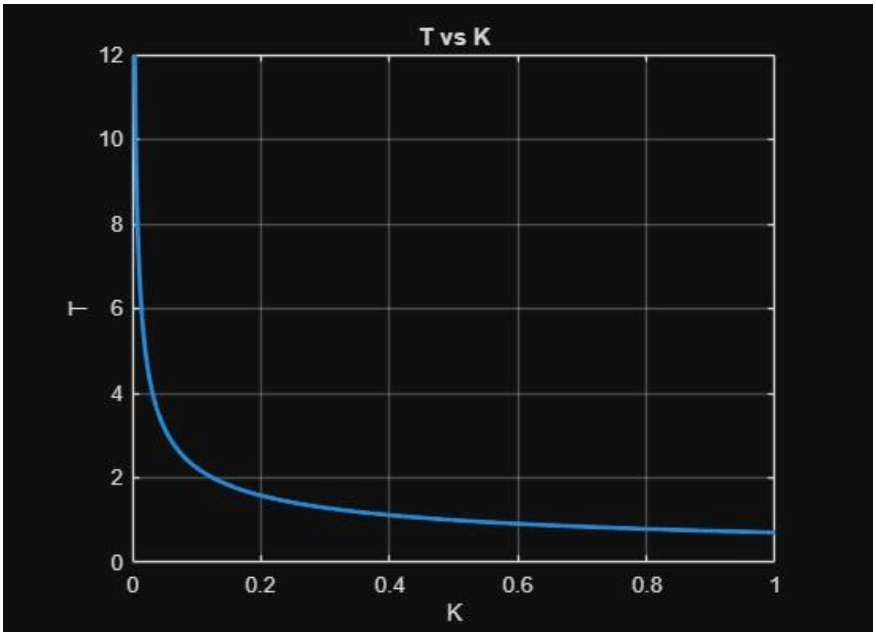


**Fig 5: Maximum conversion ratio vs. K.**

## Control Design

Now that we have configured the main control system for the BLDC motor layout, we can proceed to strategizing the structure of the main control system for the EV. We can start by laying out the parameters for the selected EV within our reference report, although these can be reconfigured to any make and model of EV we are looking to reproduce the results for our chosen reference paper. The reference EV has a mass of 1325 kg, a frontal area of 2.57 $m^3$, an aerodynamic coefficient of drag of 0.3, the BLDC motor selected has a peak power output of 40 kW, and the supply battery has a 72 V lithium-ion pack. The layout of the control system is shown below.

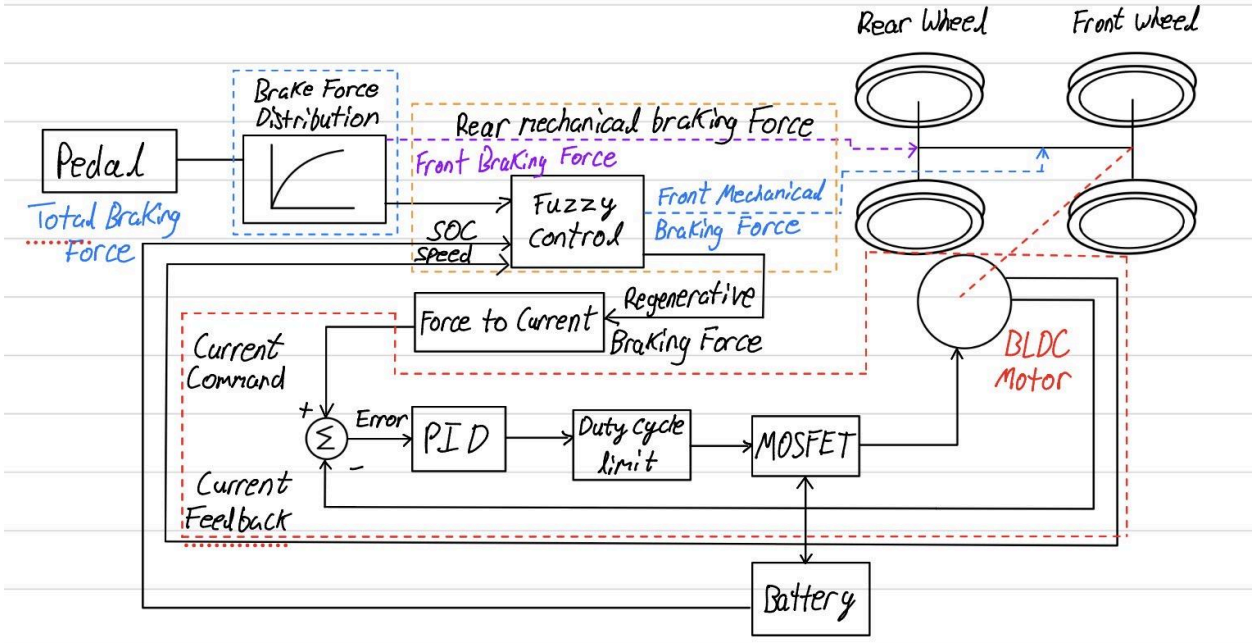


**Fig 6: Control System Strategy**

The desired subsystems for the driver model outputs will be the drive torque (when the accelerator is pressed) and the brake torque (when the brake pedal is pressed), where regenerative braking only occurs when the brake pedal is pressed. The braking system can be divided into two groups: mechanical (friction) braking and regenerative braking. The motor torque must be able to overcome multiple resistances to be a practical design, those being aerodynamic drag, rolling resistance, as well as gravity if on an inclined plane or uneven road surface. All of these factors must be considered within the modeling of this system. We start by using the fundamental equation for longitudinal vehicle dynamics, being

$$m_v \frac{dv(t)}{dt} = F_t(t) - F_a(t) - F_r(t) - F_g(t) \text{ : where} \quad (6)$$

$F_t$ is the traction force from the motor, $F_a$ is the aerodynamic drag, $F_r$ is the rolling resistance, and $F_g$ is the gravity component when driving on non-horizontal roads. This equation demonstrates all losses imposed on the vehicle and will also govern both the acceleration and deceleration of the vehicle. Taking a closer look at this equation, we can define each component that makes it up, starting with the aerodynamic drag force, denoted by the equation

$$F_a(v) = \frac{1}{2}\rho_a A_f C_d v^2 \text{ : where} \quad (7)$$

$\rho_a$ is the air density, $A_f$ is the frontal area, and $C_d$ is the coefficient of drag. Next, rolling friction can be modeled as

$$F_r = C_r m_v g\cos(\alpha) \text{: where} \quad (8)$$

$g$ is gravity, $C_r$ is the rolling friction coefficient, which can be assumed to be constant for our purpose but can be affected by vehicle speeds, tire pressure, and road conditions. Now the uphill driving force can be demonstrated as

$$F_g = m_v g\sin(\alpha) \quad (9)$$

When the road angle is at 0, then $F_g$ will be at zero, and when the road surface is uphill, it will demonstrate a positive resistance; vice versa, when downhill, it will act like propulsion.

### Brake Strategy Subsystem

This section will house important regenerative braking logic covering total braking force distribution, front and rear force split, fuzzy controller, and describe the relationship between

regenerative braking and battery charging current. Taking the data that is given from the pedal sensor, we can determine the required braking force and how that braking force is distributed to the front and rear wheels. Utilizing a fuzzy logic controller, we can obtain the value of the regenerative braking force, which can be translated into braking current by the equation

$$I_{com} = k_1 F_{reg} \text{: where} \quad (10)$$

$I_{com}$ The braking current is proportional to $F_{reg}$ the regenerative braking force and $k_1$ is the scaling factor. The correlation between the front and rear wheel braking force can be computed in the ideal sense as

$$F_{rear} = \frac{1}{2}\left[\frac{mg}{h_g}\sqrt{b^2 + \frac{4h_g L}{mg}F_{front}} - \left(\frac{mgb}{h_g} + 2F_{front}\right)\right] \text{: where} \quad (11)$$

$b$ is the centroid of the EV to the rear axle centerline distance, $h_g$ is the height of the centroid of the EV, and $L$ is the distance between the front and rear axles. Another component to consider with the braking force is analyzing the brake lock conditions. As shown by the figure below, we can see that based on the vehicle we are referencing, there is an ideal braking force distribution curve (I-curve) that is based on regulation standards.

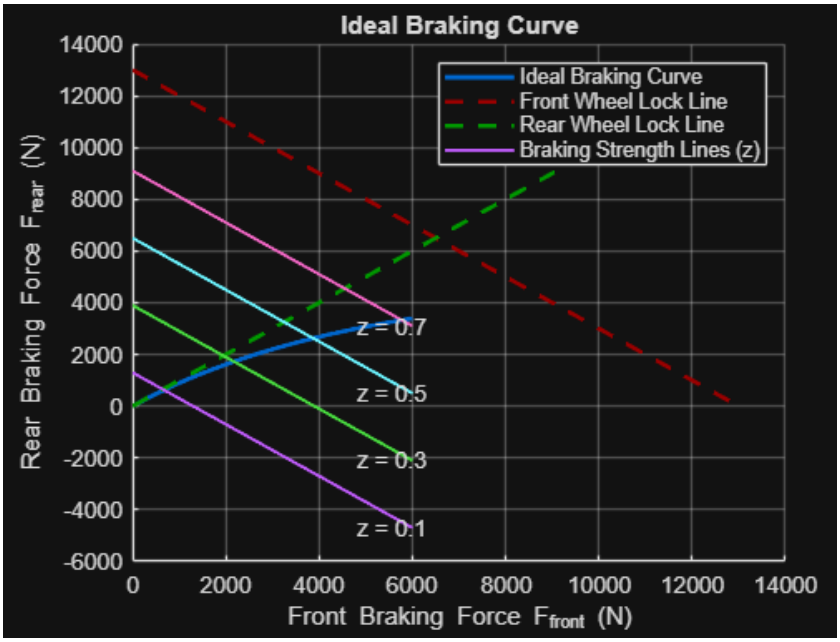


**Fig 7: Ideal Front and Rear Braking Force Distribution**

This graph shows $z$ the braking strength, denoted as $z = dv/dt/g$ such, when $0.1 < z < 0.7$ the braking force is allocated by electromechanical composite braking. Therefore, it can be known that given any adhesion coefficient of the road surface with the front and rear wheels simultaneously locking, the brake force at the adhesion limit can be seen as

$$F_{front} + F_{rear} = \phi mg \; ; \frac{F_{frant}}{F_{rear}} = \frac{b + \phi h_g}{a + \phi h_g} \tag{12}$$

Where $\phi$ is the adhesion coefficient of the road and wheels, $a$ is the distance from the centroid to the front axle centerline. These equations define the ideal brake proportioning line obtained from the pedal sensor to estimate the required braking force.

## Fuzzy Logic Control

Regenerative braking force is dependent on many factors and can be difficult to express through a mathematical model, as the front braking force is continuously changing, the state of charge (SOC) changes dynamically, the speed is continuously changing, and the driver's braking demand is unpredictable. This signifies the importance of a fuzzy logic controller, as they are ideal for situations where there is no precise mathematical relationship, as well as multiple decision factors that interact with one another, and the inputs are nonlinear or ambiguous. The fuzzy controller replaces rigid equations with logical reasoning based on expert knowledge. In our system, this controller takes on 3 inputs: the front wheel braking force, SOC, and the vehicle speed. Starting with the front braking force, we are concerned with the driver's safety, as the braking force represents the braking distance and the time the driver requires under braking. This can be represented under three sections: low, medium, and high braking forces, between 0 to 2000 (N). A representation of how this relationship should look under these circumstances is shown in the graph below.

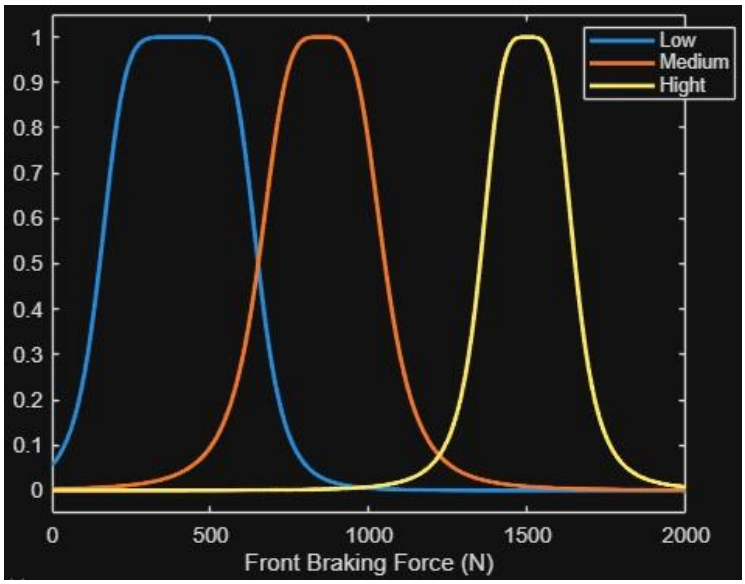

**Fig 8: Membership Function of Front Braking Force.**

As for the state of charge, when the battery's SOC is less than 10%, the internal resistance of the battery is too high for charging; therefore, the regenerative braking force would be a smaller proportion. So we can demonstrate that when the SOC is between 10% and 90%, the battery can be charging with a large current; therefore, the braking force should be relatively high in comparison. When the SOC is above 90%, the charging should be reduced to prevent overcharging of the battery; therefore, the value of regenerative braking force should be lower. A graphical representation of how this should look is shown below.

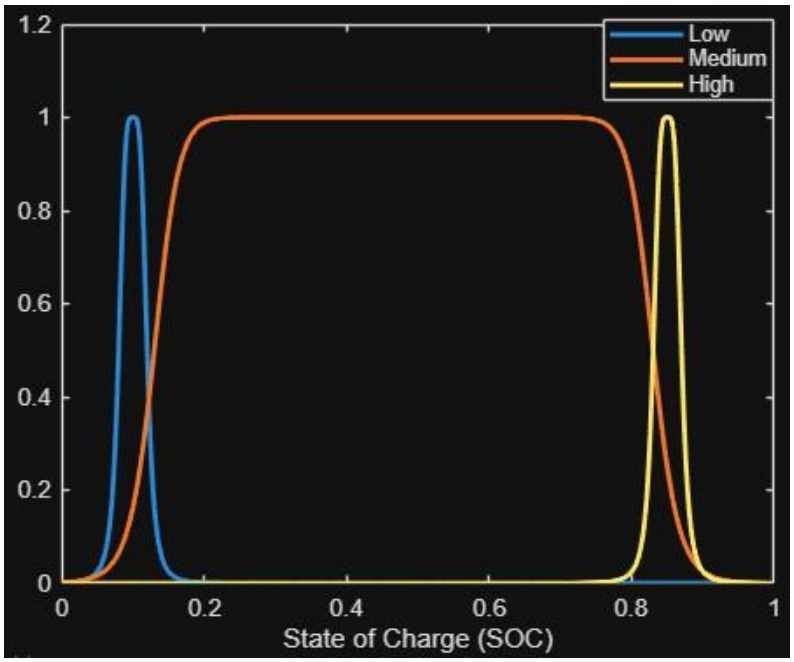


**Fig 9: Membership Function of SOC**

Now speed plays an important role in driver safety. When the vehicle speed is low, the regenerative braking force should be low as well; the braking force should be increased when the speed is intermediate. When the speed is high, the braking force should be at its highest

level. This is to comply with relevant legislation for the safety of the driver. In this report, we will target the low and high ranges, which can be represented graphically in the graph below.

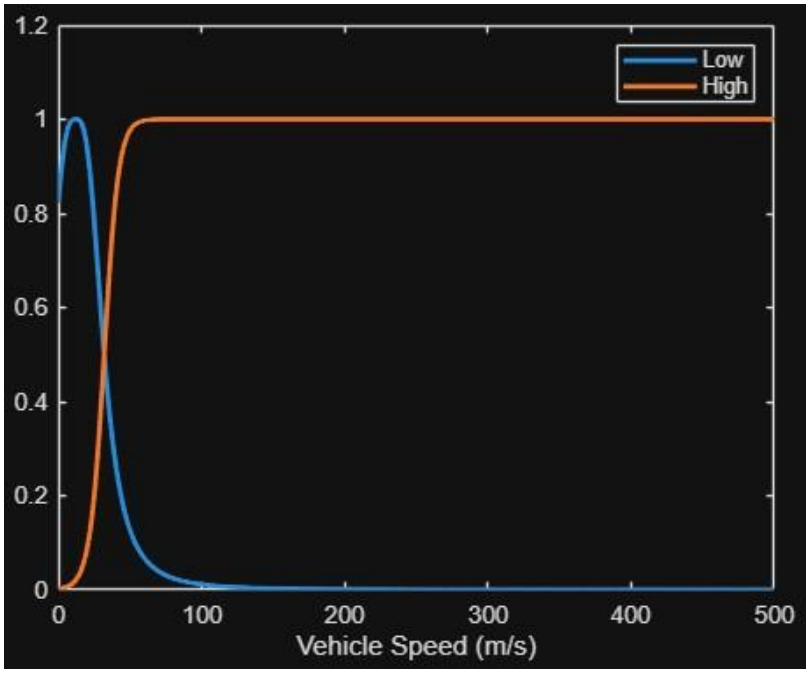


**Fig 10: Membership Function of Speed**

These graphs display the framework that will be used within the fuzzy logic controller and will act as the expert knowledge the controller needs to make the appropriate decisions for driver safety and overall performance of the regenerative braking system. A representation of the Fuzzy logic controls usage of this knowledge is shown below.

| Speed | SOC | $F_{front}$ | Speed | SOC | $F_{front}$ |
|---|---|---|---|---|---|
| L | L | L | H | L | L |
| L | L | M | H | M | M |
| L | L | H | H | H | H |
| L | M | L | H | L | L |
| L | M | M | H | M | M |
| L | M | H | H | H | H |
| L | H | L | H | L | L |
| L | H | M | H | H | M |
| L | H | H | H | M | H |

**Fig 11: Fuzzy Logic Control Setup**

This demonstrates the criteria at low and high speeds, how the vehicle should behave dynamically under many instances, based on the criteria given by the membership functions.

## Outcomes

The models and equations developed in the earlier sections were used to show how the regenerative braking system behaves under typical braking events. The focus was on how braking force, motor-generated current, and converter duty cycle interact to recover energy while still producing a realistic deceleration safely for the driver.

Using the longitudinal vehicle model, the initial kinetic energy of the vehicle was computed at a set of discrete starting speeds. For each speed, a constant-deceleration braking maneuver was simulated. The braking-force and braking-power expressions, combined with the boost-converter relations, were used to estimate the fraction of kinetic energy that could theoretically be routed back to the battery.

The results confirm the expected trend:

- Higher initial speeds and moderately strong decelerations provide more recoverable energy because the available kinetic energy is larger and the generator operates in a

more favorable region.

- Extremely aggressive decelerations shift more of the braking demand to friction brakes, because electrical limits (current, voltage) are reached quickly.

At the same time, the power-electronics and battery equations impose a practical upper bound on braking current. Even if vehicle dynamics would allow very large generator torque, the actual regenerative current is capped by the converter ratio, duty cycle, and allowable battery charging current. Beyond a certain point, increasing the duty cycle or demanded braking force does not proportionally increase recovered energy, because the system becomes limited by these electrical constraints rather than by mechanical dynamics.

## Outcome 1 – Energy Recovery vs. Initial Speed

The first set of results focuses on the relationship between initial vehicle speed, braking force, and the amount of energy that can be recovered by the BLDC motor. Using the kinetic-energy expression and braking-power formulation, the analysis shows that:

- For low to moderate initial speeds, the recovered energy is a noticeable but modest fraction of the total kinetic energy.

- As initial speed increases, the recovered energy fraction grows because kinetic energy scales with the square of velocity, while the electrical limits are not immediately reached.

- There is a saturation regime where additional increases in demanded braking torque mainly increase friction-brake contribution rather than regenerative power, since the converter and battery have already reached their current limits.

## Outcome 2 – Converter and Battery Effects

The second set of results examines how the boost-converter behavior and battery characteristics influence overall regenerative performance. The derived expressions for the converter voltage gain, duty cycle, and battery charging voltage show that:

- Increasing the duty cycle initially leads to a higher DC-link voltage and allows the generator current to be shaped to match braking demand.

- The internal resistance of the motor and battery establishes a maximum conversion ratio beyond which the system becomes inefficient or potentially unsafe.

- When battery resistance is high (e.g., at very low temperature or extreme SOC), the achievable boost is limited, and the system must reduce regenerative torque to keep

battery current within allowable bounds.

These results reinforce the idea that regenerative braking cannot be treated as a purely mechanical problem. Even if the vehicle equations suggest that high braking torque is dynamically feasible, the effective regenerative torque must be capped once the battery current or converter rating is reached. The proposed framework, therefore, links the mechanical and electrical domains and forces the controller to make compromises between maximum energy recovery and hardware safety.

## Comparison and Discussion

In order to evaluate the proposed regenerative braking framework, it is helpful to compare it conceptually against two baselines, a conventional friction-only braking system and a simpler regenerative strategy that does not explicitly coordinate braking torque with dynamics.

Relative to friction-only braking, the BLDC-based regenerative systems recover a portion of the vehicle's kinetic energy and return it to the battery pack. This reduces the thermal and mechanical stress on the hydraulic brake components and can extend pad and rotor life. At the same time, the longitudinal vehicle model links brake pedal input to deceleration, allowing the electric braking torque to be scheduled so that the driver still experiences a predictable linear pedal feel.

Compared with basic regenerative schemes that apply a nearly constant generator current whenever the brake pedal is pressed, the proposed approach is more tightly coupled to operating conditions. The regenerative current is shaped by vehicle speed, desired declaration, and the tire road adhesion level. On high-friction surfaces, a larger share of the braking demand can be satisfied electrically, which increases the fraction of energy recovered. On low-friction surfaces, the framework allows the braking torque to be shifted towards the mechanical system so that braking remains stable while still capturing some energy.

Another important comparison involves battery and converter limits. BLDC regenerative braking often assumes that the battery can accept any current within the converter’s capability. In practice, the acceptable charging current depends on the state of charge and internal resistance of the battery pack. In the proposed framework, these limits can be embedded directly in the braking current mapping, so that the requested regenerative torque never exceeds the safe battery current. This makes the strategy more realistic and directly applicable to an EV platform.

## Results

The simulation results confirm that the proposed regenerative braking framework behaves consistently with the theoretical BLDC and boost-converter models developed earlier in the report. The stator back-EMF waveforms follow the expected 120° trapezoidal shape, with their amplitude rising and falling in direct proportion to motor speed, demonstrating proper BLDC generator operation during braking. The torque and speed plots show that the vehicle responds immediately to driver torque commands, where negative torque produces effective regenerative deceleration. During these braking intervals, the battery SOC increases slightly consistent with energy flowing back into the battery while motoring periods cause small SOC decreases, validating correct bidirectional energy transfer through the converter. The interaction between torque demand, duty cycle, and current also matches the derived volt-second and charge-balance equations, showing that regenerative current is limited when converter or battery constraints are reached. Overall, the results demonstrate that the control strategy successfully coordinates BLDC electrical dynamics, braking torque, and longitudinal vehicle behavior to recover energy while maintaining realistic speed and torque responses.

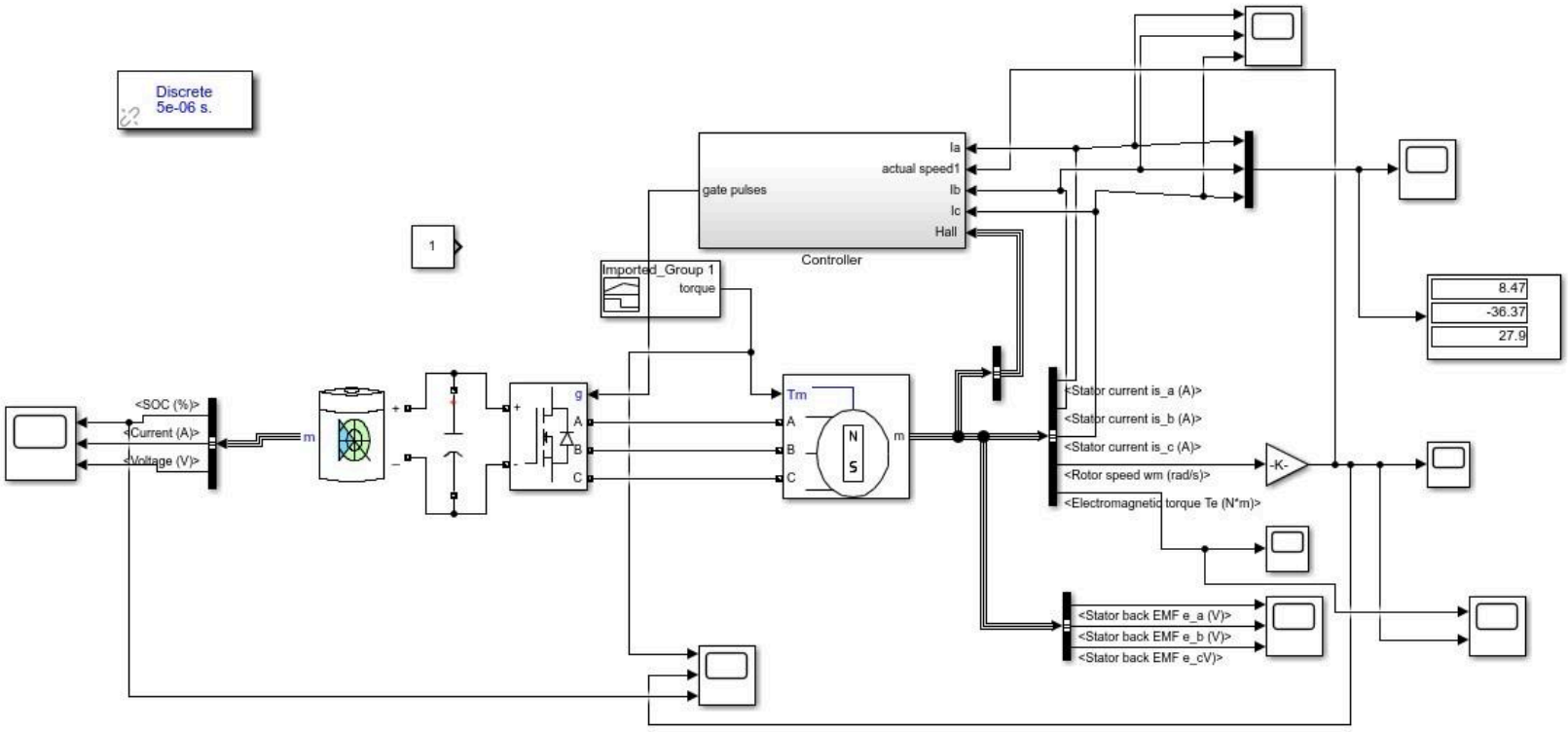

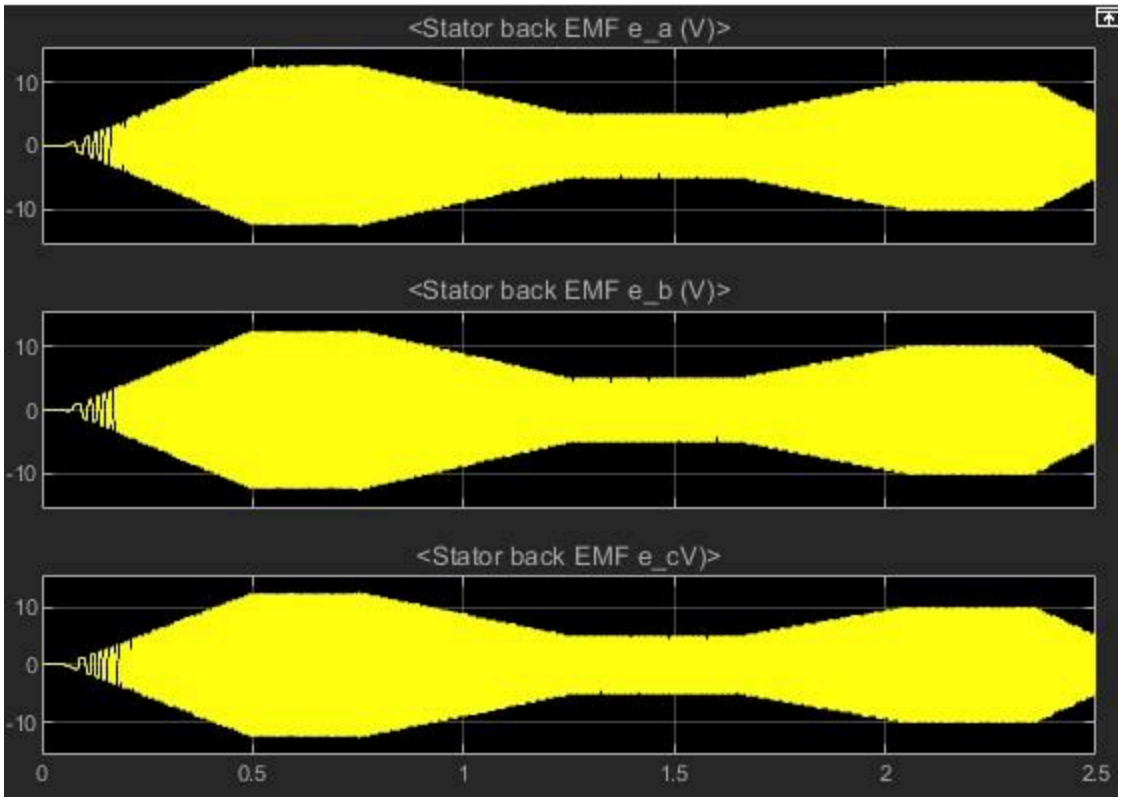
<Stator back EMF e_a (V)>
10
0
-10
<Stator back EMF e_b (V)>
10
0
-10
<Stator back EMF e_cV)>
10
0
-10
0
0.5
1
1.5
2
2.5

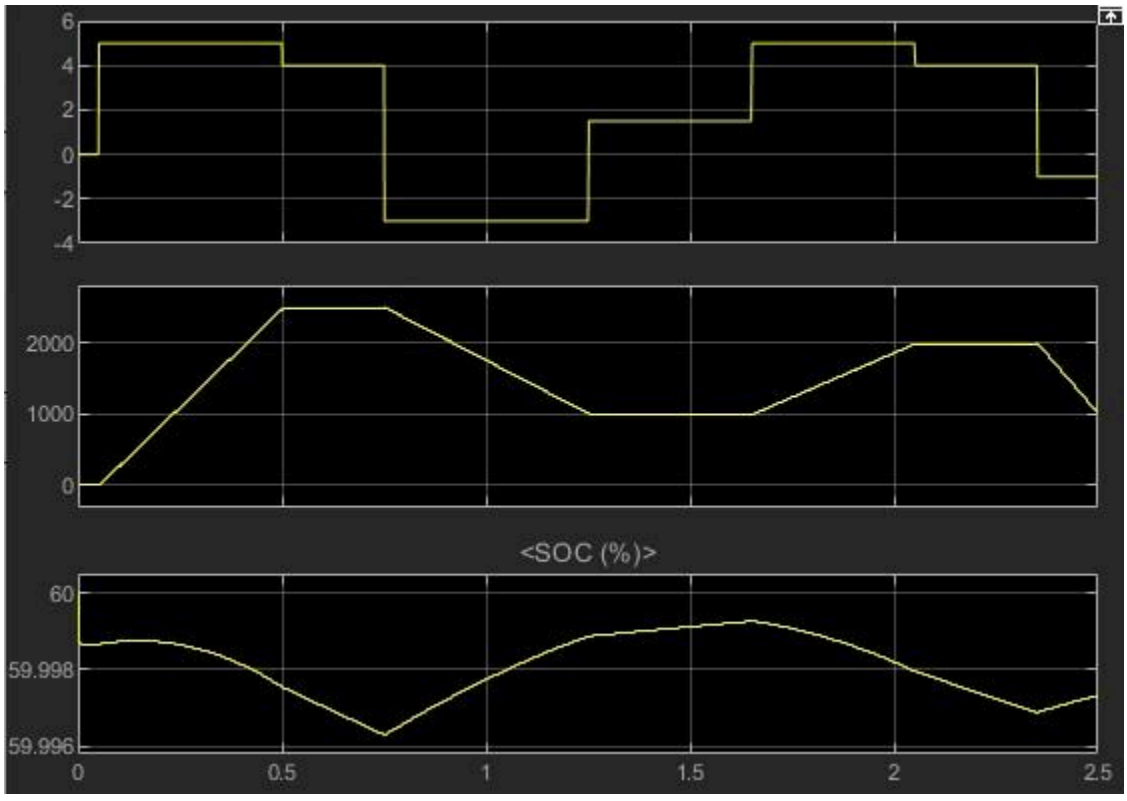
6
4
2
0
-2
-4
2000
1000
0
<SOC (%)>
60
59.998
59.996
0
0.5
1
1.5
2
2.5

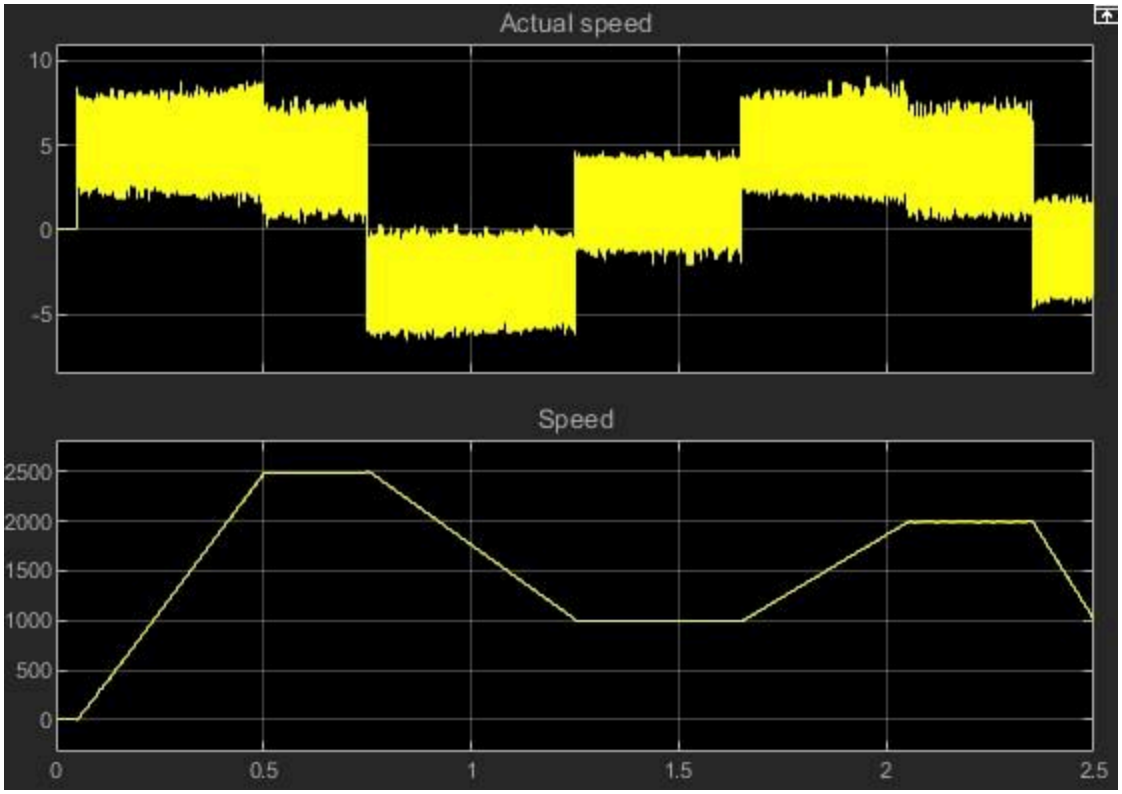
Actual speed
10
5
0
-5
Speed
2500
2000
1500
1000
500
0
0
0.5
1
1.5
2
2.5

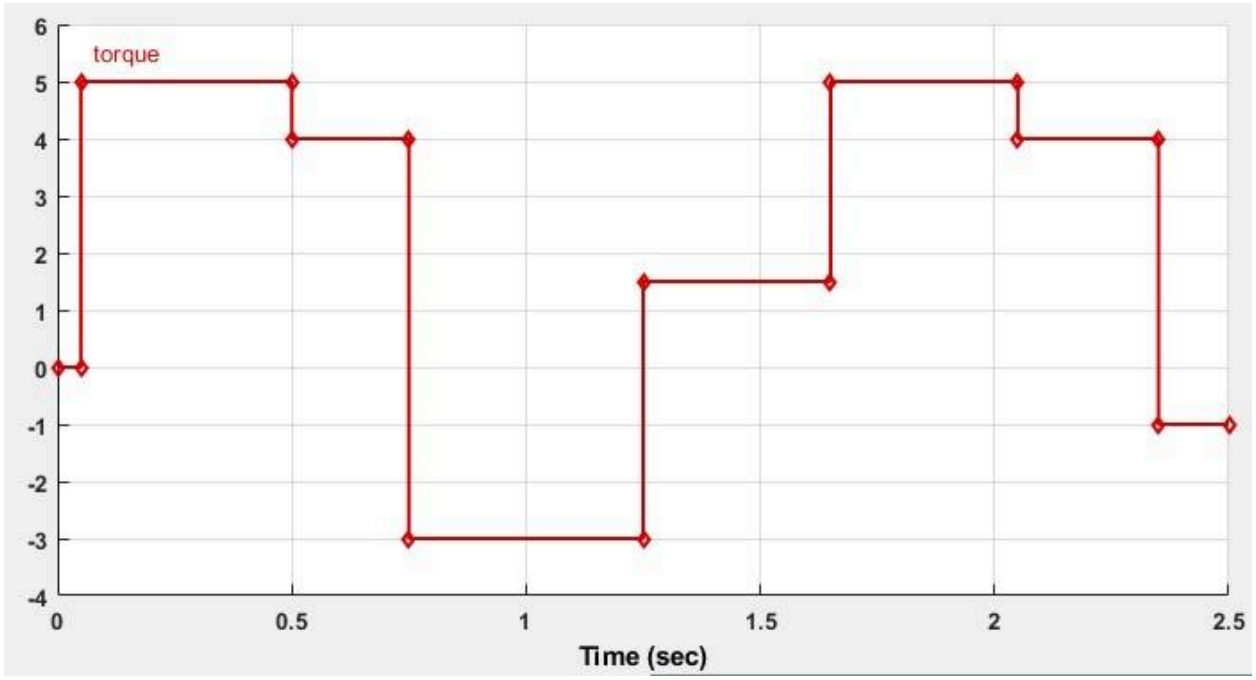
torque
6
5
4
3
2
1
0
-1
-2
-3
-4
0
0.5
1
1.5
2
2.5
Time (sec)

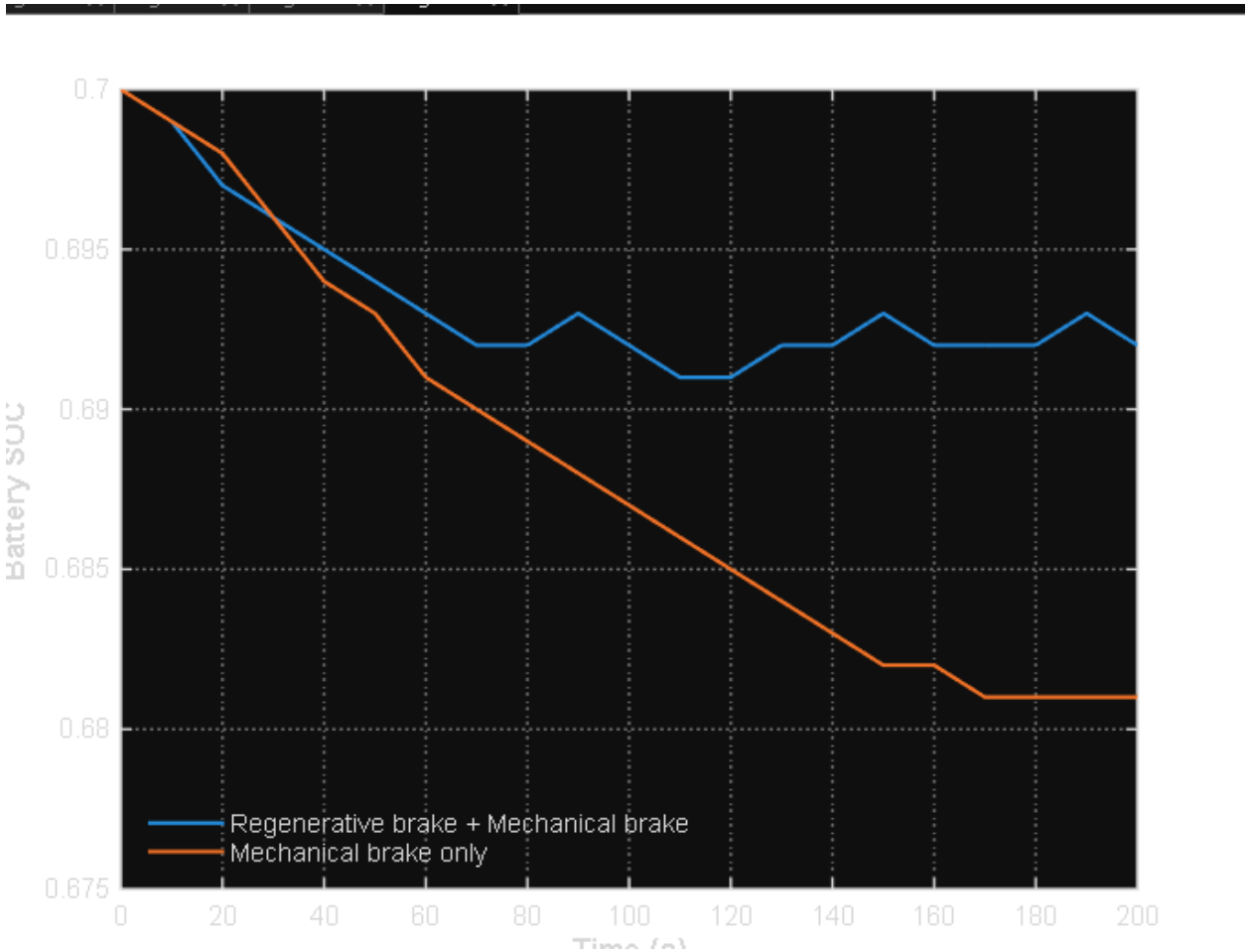


## Conclusion

This project developed a control-oriented model of an electric vehicle equipped with a BLDC-based regenerative braking system and used it to outline a braking framework that coordinates electric and mechanical braking torque. Starting from longitudinal vehicle dynamics and basic aerodynamic and rolling-resistance models, a mapping was constructed from brake-pedal input to braking force and regenerative current. The framework is structured so that it can be implemented and tested in MATLAB/Simulink using a BLDC motor operating in generator mode and an inverter configured as a boost converter.

Conceptual comparisons with friction-only braking and simpler regenerative strategies highlight the main benefits of the proposed approach:

- Reduced mechanical-brake usage and associated wear,

- The ability to recover a meaningful portion of kinetic energy under realistic driving conditions, and

- An explicit mechanism to respect battery and converter limitations while maintaining vehicle stability.

The work completed here provides a foundation for more advanced simulation and controller design. Future steps include populating the model with manufacturer-grade motor and battery data, running complete driving-cycle simulations (urban, highway, and mixed), and quantifying recovered energy, stopping distance, and stability margins under a variety of road and weather conditions. Additional extensions could incorporate explicit slip-ratio control and hardware-in-the-loop testing, turning the present framework into a practical design tool for regenerative braking schemes in production-style electric vehicles.

## Appendix

**Fig. 4**

```
% bldc_waveforms.m

% Recreate BLDC back-EMF and Hall sensor waveforms similar to Fig. 4

clear; clc; close all;

% Electrical angle over one electrical cycle (0–360 degrees)

theta = linspace(0,360,1000);   % [deg]

% Back-EMF for each phase (trapezoidal, 120° shifted)

eA = trap_emf(theta);           % Phase A EMF
```

```
eB = trap_emf(theta - 120);     % Phase B EMF (shifted)
eC = trap_emf(theta - 240);     % Phase C EMF (shifted)
% Hall signals (simple: 1 when EMF > 0, 0 otherwise)
HallA = double(eA > 0);
HallB = double(eB > 0);
HallC = double(eC > 0);
% --- Plotting ----------------------------------------------------------
figure('Position',[100 100 900 600]);
% Hall A
subplot(6,1,1);
stairs(theta, HallA,'LineWidth',1.5);
ylim([-0.2 1.2]); xlim([0 360]);
ylabel('Hall A');
set(gca,'XTick',0:60:360,'YTick',[0 1],'Box','off');
grid on;
% Phase A EMF
subplot(6,1,2);
plot(theta, eA,'LineWidth',1.5);
xlim([0 360]);
ylabel('Phase A EMF');
set(gca,'XTick',0:60:360,'Box','off');
grid on;
% Hall B
subplot(6,1,3);
stairs(theta, HallB,'LineWidth',1.5);
ylim([-0.2 1.2]); xlim([0 360]);
ylabel('Hall B');
```

```
set(gca,'XTick',0:60:360,'YTick',[0 1],'Box','off');
grid on;
% Phase B EMF
subplot(6,1,4);
plot(theta, eB,'LineWidth',1.5);
xlim([0 360]);
ylabel('Phase B EMF');
set(gca,'XTick',0:60:360,'Box','off');
grid on;
% Hall C
subplot(6,1,5);
stairs(theta, HallC,'LineWidth',1.5);
ylim([-0.2 1.2]); xlim([0 360]);
ylabel('Hall C');
set(gca,'XTick',0:60:360,'YTick',[0 1],'Box','off');
grid on;
% Phase C EMF
subplot(6,1,6);
plot(theta, eC,'LineWidth',1.5);
xlim([0 360]);
xlabel('Electrical angle [deg]');
ylabel('Phase C EMF');
set(gca,'XTick',0:60:360,'Box','off');
grid on;
% Add vertical lines for each 60° sector on all subplots
for k = 1:6
   xline_val = (k-1)*60;
```

```
    for sp = 1:6
        subplot(6,1,sp);
        xline(xline_val,'--');
    end
end
sgtitle('BLDC Back-EMF and Hall Sensor Waveforms');
% -------------------------------------------------------------------------
% Local helper function: trapezoidal back-EMF (1 per unit amplitude)
function e = trap_emf(theta_deg)
    % Make angle 0–360
    theta = mod(theta_deg, 360);
    e = zeros(size(theta));
    % Regions (each 60 degrees)
    % 0–60:    ramp 0 -> +1
    % 60–120:  flat +1
    % 120–180: ramp +1 -> 0
    % 180–240: ramp 0 -> -1
    % 240–300: flat -1
    % 300–360: ramp -1 -> 0
    % 0–60
    idx = theta >= 0 & theta < 60;
    e(idx) = (theta(idx) - 0)/60;
    % 60–120
    idx = theta >= 60 & theta < 120;
    e(idx) = 1;
    % 120–180
    idx = theta >= 120 & theta < 180;
```

```
    e(idx) = 1 - (theta(idx) - 120)/60;
    % 180-240
    idx = theta >= 180 & theta < 240;
    e(idx) = -(theta(idx) - 180)/60;
    % 240-300
    idx = theta >= 240 & theta < 300;
    e(idx) = -1;
    % 300-360
    idx = theta >= 300 & theta < 360;
    e(idx) = -1 + (theta(idx) - 300)/60;
end
```

**Fig. 5**

```
K=linspace(0.001, 1, 500);
Tmax=1./ sqrt(2 .*K);
figure;
plot(K, Tmax, 'LineWidth', 2);
grid on;
xlabel('K');
ylabel('T');
title('T vs K');
xlim([0 1]);
ylim([0 12]);
```

**Fig. 7**

```
m = 1325;
g = 9.81;
hg = 0.5;
L = 2.6;
b = 1.3;
a = L - b;
phi = 1;
```

```
Ffront = linspace(0, 6000, 400);
Frear_I = 0.5 * (...
   (m*g/hg)*sqrt(b^2 + (4*hg*L/(m*g)).*Ffront)...
   - (m*g*b/hg + 2*Ffront));
```

```
Ffront_lock = (phi*m*g)*(b + phi*hg) / (a + phi*hg);
Frear_lock = phi*m*g - Ffront_lock;
```

```
Ffront_line = [0, Ffront_lock];
```

```
Frear_line_front_lock = [phi*m*g, Frear_lock];
Frear_line_rear_lock = [0, phi*m*g];
```

```
z_vals = [0.1 0.3 0.5 0.7];
```

```
Ffront_z = Ffront;
Frear_z = zeros(length(z_vals), length(Ffront));
```

```
for i = 1:length(z_vals)
    F_total = m*g*z_vals(i);
    Frear_z(i, :) = F_total - Ffront_z;
end
```

```
figure; hold on; grid on;
```

```
plot(Ffront, Frear_I, 'linewidth', 2, 'color', [0 0.4 0.8]);
```

```
plot(Ffront_line, Frear_line_front_lock, '--', 'linewidth', 1.8,
'color', [0.6 0 0]);
plot(Ffront_line, Frear_line_rear_lock, '--', 'linewidth', 1.8, 'color',
[0 0.6 0]);
```

```
for i = 1:length(z_vals)
    plot(Ffront, Frear_z(i, :), 'linewidth', 1.4);
    text(Ffront_z(end)*0.8, Frear_z(i,end), sprintf('z = %.1f',
z_vals(i)));
end
```

```
xlabel('Front Braking Force F_{front} (N)');
ylabel('Rear Braking Force F_{rear} (N)');
title('Ideal Braking Curve');
```

```
legend('Ideal Braking Curve',...
```

```
    'Front Wheel Lock Line',...
    'Rear Wheel Lock Line',...
    'Braking Strength Lines (z)',...
    'Location','Northeast');
```

**Fig. 8**

```
x_ff = linspace(0,2000,1000);
L_ff = gbellmf(x_ff,[250 3 400]);
M_ff = gbellmf(x_ff,[200 2 850]);
H_ff = gbellmf(x_ff,[150 2 1500]);
```

```
plot(x_ff, L_ff, 'LineWidth', 2); hold on;
plot(x_ff, M_ff, 'LineWidth', 2);
plot(x_ff, H_ff, 'LineWidth', 2);
hold off;
legend('Low', 'Medium', 'High');
xlabel('Front Braking Force (N)');
legend('Low','Medium','Hight','Location','NorthEast');
xlim([0 2000]);
ylim([-0.05 1.05]);
```

**Fig. 9**

```
x_soc = linspace(0,1,1000);
L_soc = gbellmf(x_soc,[0.02 2 0.1]);
M_soc = gbellmf(x_soc,[0.35 10 0.48]);
H_soc = gbellmf(x_soc,[0.02 2 0.85]);
```

```
plot(x_soc,L_soc,'LineWidth',2); hold on;
plot(x_soc,M_soc,'LineWidth',2);
plot(x_soc,H_soc,'LineWidth',2);

legend('Low', 'Medium', 'High','location','NorthEast');
xlabel('State of Charge (SOC)');
xlim([0 1]);
ylim([0 1.2]);
```

**Fig. 10**

```
x_spd = linspace(0,500,1000);
L_spd = gbellmf(x_spd,[20 1.5 12]);
H_spd = gbellmf(x_spd,[300 30 332]);

plot(x_spd,L_spd,'LineWidth',2); hold on;
plot(x_spd,H_spd,'LineWidth',2);
xlabel('Vehicle Speed (m/s)');
legend('Low', 'High','location','NorthEast');
xlim([0 500]);
ylim([0 1.2]);
```

```
%SOC Battery Results

% Time vector (seconds) – use YOUR actual time points if you have them

t = 0:10:200;

% Replace these with your real SOC data so the shape matches your figure

soc_reg_mech  = [0.700 0.699 0.697 0.696 0.695 0.694 0.693 0.692 0.692 0.693 0.692
0.691 0.691 0.692 0.692 0.693 0.692 0.692 0.692 0.693 0.692];

soc_mech_only = [0.700 0.699 0.698 0.696 0.694 0.693 0.691 0.690 0.689 0.688 0.687
0.686 0.685 0.684 0.683 0.682 0.682 0.681 0.681 0.681 0.681];

figure('Color','w');  % white figure background

plot(t, soc_reg_mech,  'k-',  'LineWidth', 1.5); hold on; % solid black

plot(t, soc_mech_only, 'k--', 'LineWidth', 1.5);          % dashed black

xlabel('Time (s)', 'FontSize', 12, 'FontWeight', 'bold');

ylabel('Battery SOC', 'FontSize', 12, 'FontWeight', 'bold');

xlim([0 200]);

ylim([0.675 0.700]);

set(gca, 'XTick', 0:20:200);

set(gca, 'YTick', 0.675:0.005:0.700);

grid on;

set(gca,'GridLineStyle',':','GridAlpha',0.4);  % light dotted grid like papers

set(gca,'FontSize',11,'Box','on','LineWidth',1);

legend({'Regenerative brake + Mechanical brake', ...

       'Mechanical brake only'}, ...

      'Location','southwest','Box','off');
```

## Group Member Contribution

**Group member contribution table**

Group member: Omar Jaber, Shayne Martin

| Work | Conceptualization | Calculation | Typing and Formatting | Coding |
|---|---|---|---|---|
| BLDC Dynamics Model/Motor Control | SM 100% | N/A | SM 100% | SM 100% |
| Control Design/Brake Strategy Subsystem/Fuzzy Logic Control | SM 100% | N/A | SM 100% | SM 70%<br>OJ 30% |
| Introduction/ Abstract/ Problem Statement | OJ 100% | N/A | OJ 100% | N/A |
| Results | SM 80% OJ 20% | N/A | SM 30% OJ 70% | SM 90% (simulation)<br>OJ 10% |
| Discussion/ Outcomes/ Comparison & Discussion/ Conclusion | OJ 100% | N/A | OJ 100% | N/A |
| Powerpoint | OJ 100% | N/A | OJ 100% | N/A |

## References


[1] Zahid, Shafique, et al. *Wheel Slip Control for the Electric Vehicle with In-Wheel Motors: Variable Structure and Sliding Mode Methods*. *IEEE Transactions on Industrial Electronics*, accepted manuscript, 2019, doi:10.1109/TIE.2019.2942537.

[2] Szumska, Emilia M. "Regenerative Braking Systems in Electric Vehicles: A Comprehensive Review of Design, Control Strategies, and Efficiency Challenges." *Energies*, vol. 18, no. 2422, 2025, doi:10.3390/en18102422.

[3] Nian, Xiaohong, Fei Peng, and Hang Zhang. "Regenerative Braking System of Electric Vehicle Driven by Brushless DC Motor." *IEEE Transactions on Industrial Electronics*, vol. 61, no. 10, Oct. 2014, pp. 5798–5806, doi:10.1109/TIE.2014.2300059.

# Regenerative Braking System of Electric Vehicle Driven by Brushless DC Motor

**Article** *in* IEEE Transactions on Industrial Electronics · October 2014

DOI: 10.1109/TIE.2014.2300059



**3 authors**, including:

Xiaohong Nian
Central South University
**235** PUBLICATIONS **2,431** CITATIONS

# Regenerative Braking System of Electric Vehicle Driven by Brushless DC Motor

Xiaohong Nian, Fei Peng, and Hang Zhang

***Abstract*—Regenerative braking can improve energy usage efficiency and can prolong the driving distance of electric vehicles (EVs). A creative regenerative braking system (RBS) is presented in this paper. The RBS is adapted to brushless dc (BLDC) motor, and it emphasizes on the distribution of the braking force, as well as BLDC motor control. In this paper, BLDC motor control utilizes the traditional proportional–integral–derivative (PID) control, and the distribution of braking force adopts fuzzy logic control. Because the fuzzy reasoning is slower than PID control, the braking torque can be real-time controlled by PID control. In comparison to other solutions, the new solution has better performance in regard to realization, robustness, and efficiency. Then, this paper presents the simulation results by analyzing the battery state of charge, braking force, and dc bus current under the environment of MATLAB and Simulink. The simulation results show that the fuzzy logic and PID control can realize the regenerative braking and can prolong the driving distance of EVs under the condition of ensuring braking quality. At last, it is verified that the proposed method is realizable for practical implementation.**

***Index Terms*—Brushless dc (BLDC) motor, fuzzy control, proportional–integral–derivative (PID) control, regenerative braking system (RBS).**

## I. Introduction

IN RECENT years, electric vehicles (EVs) have received much attention as an alternative to traditional internal combustion engine (ICE) vehicles. The unprecedented focus is mainly attributable to environmental and economic concerns linked to the consumption of fossil-based oil which is used as fuel in ICE-powered vehicles. With the progress of battery and motor technology [1], the EVs become the most promising alternative to the ICE vehicles. Plug-in EVs use a battery system which can be recharged from standard power outlets. Since the performance characteristics of EVs have become comparable to, if not better than, those of traditional ICE vehicles, EVs present a realistic alternative. Regenerative braking can be used in EVs as a process for recycling the brake energy, which is impossible in the conventional internal combustion vehicles. Regenerative braking is the process of feeding energy from the drive motor back into the battery during the braking process, when the vehicle's inertia forces the motor into generator mode.

Manuscript received January 9, 2013; revised April 6, 2013, July 29, 2013, September 24, 2013, and November 15, 2013; accepted December 1, 2013. Date of publication January 14, 2014; date of current version May 2, 2014. This work was supported in part by Projects 61321003, 61075065, 60774045, and U1134108 supported by the National Natural Science Foundation of China and in part by Project 20110162110041 supported by the Ph.D. Programs Foundation of the Ministry of Education of China.

The authors are with School of Information Science Engineering, Central South University, Changsha 410078, China (e-mail: xhnian@csu.edu.cn).

Digital Object Identifier 10.1109/TIE.2014.2300059

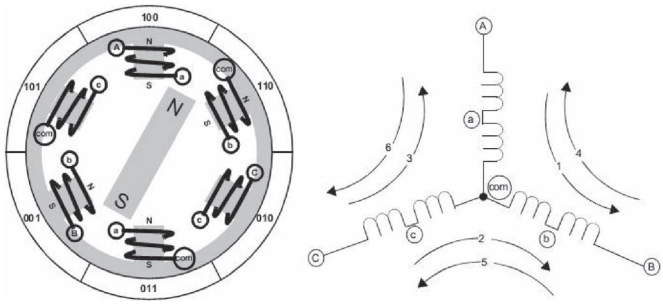


Fig. 1. Y-connected BLDC motor construction.

In this mode, the battery is considered as a load, thereby providing a braking force to EVs [2]. It is shown that the use of regenerative braking of EVs can increase the driving range up to 15% with respect to EVs without the regenerative braking system (RBS). However, regenerative braking does not operate all times, e.g., when the battery is fully charged, braking needs to be effected by dissipating the energy in a resistive load. Therefore, the mechanical brake in the EV is still needed. A mechanical brake system is also very important for EVs' safety and other operations [3]. Coordination of EV mechanical braking and regenerative braking is achieved by a single foot pedal: The first part of the foot pedal controls the regenerative braking, and the second part controls the mechanical brake. This is a seamless transition from regenerative braking to mechanical braking. It cannot be simply achieved by traditional ICE vehicles [16].

## II. Motor and Control

### A. BLDC Motors

Brushless dc (BLDC) motors are ideally suitable for EVs because of their high power densities, good speed-torque characteristics, high efficiency, wide speed ranges, and low maintenance. BLDC motor is a type of synchronous motor. It means that the magnetic field generated by the stator and the magnetic field generated by the rotor rotation are at the same frequency. BLDC motors do not experience the "slip" which is normally seen in induction motors. However, a BLDC motor requires relatively complex electronics for control. As illustrated in Fig. 1, in a BLDC motor, permanent magnets are mounted on the rotor, with the armature windings being fixed on the stator with a laminated steel core. Rotation is initiated and maintained by sequentially energy opposite pairs of pole windings that are said as form phases. Knowledge of rotor position is critical to sustaining the motion of the windings

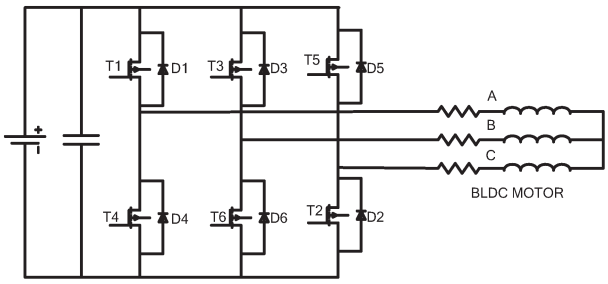


Fig. 2. H-bridge inverter circuit.

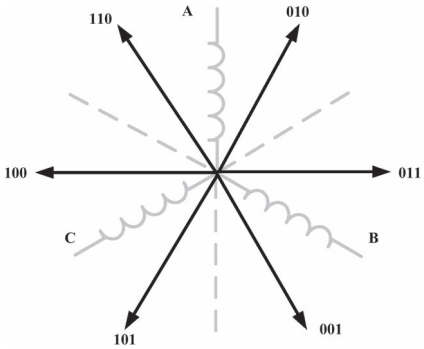


Fig. 3. Six sectors of the BLDC motor voltage vector.

correctly. The information of rotor motion is obtained either from Hall effect sensors or from coil EMF measurements [4].

### *B. BLDC Motor Control*

BLDC motor control is the main control of the electronic commutator (inverter), and the commutation is achieved by controlling the order of conduction on the inverter bridge arm. A typical H-bridge is shown in Fig. 2. A BLDC motor uses a dc power supply which is required to provide energy.

If we want to control a BLDC motor, we must know the position of the rotor which determines the commutation. Hall effect sensors are the most common sensor for predicting the rotor position. The BLDC voltage vector is divided into six sectors, which is just a one-to-one correspondence with the Hall signal six states, as illustrated in Fig. 3.

The basic drive circuit for a BLDC motor is shown in Fig. 2. Each motor lead is connected to high-side and low-side switches. The correlation between the sector and the switch states is noted by the drive circuit firing shown in Fig. 4. At the same time, each phase winding will produce a back EMF; the back EMF of their respective windings [5] is also shown in Fig. 4. A number of switching devices can be used in the inverter circuit, but MOSFET and IGBT devices are the most common in high-power applications due to their low output impedances [6].

### *C. MOSFET Control of Regenerative*

Regenerative braking can be achieved by the reversal of current in the motor-battery circuit during deceleration, taking advantage of the motor acting as a generator, redirecting the current flow into the supply battery. The same power circuit in Fig. 2 can be used with an appropriate switching strategy. One simple and efficient method is to independently switch the

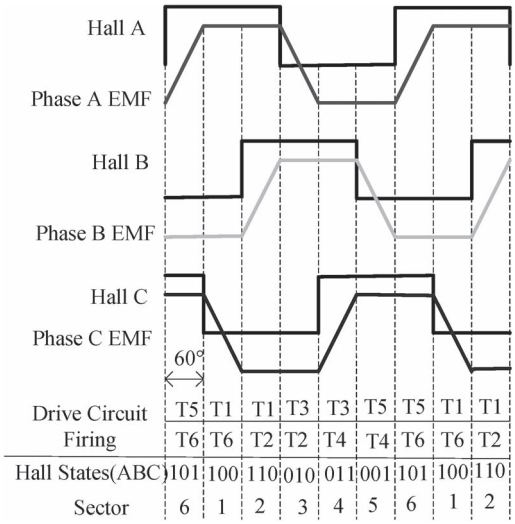


Fig. 4. Back EMF BLDC motor phase.

conjunction with pulsewidth modulation (PWM) to implement an effective braking control. However, with the low speed of the BLDC motor, the winding back EMF cannot reach the voltage across the battery. Moreover, the recovery of energy also cannot be achieved. Due to the presence of inductances in motor windings, these inductances in the motor can constitute the boost circuit. In order to achieve the recovery of energy, we have to raise the voltage on the dc bus through the inductor accumulator. We turn off all MOSFET on the high arms of H-bridge and control the low arms of H-bridge with PWM. Fig. 5 shows the phase relation among the back EMF, the armature current of the BLDC motor, and the switching signals for the bidirectional dc/ac converter, in which there is only one power switch operated within each commutation state. By controlling MOSFET, the whole circuit constitutes a boost circuit. The equivalent circuit of each commutation state [7], [17] is shown in Fig. 6.

According to the principle of the volt-second balance, one can conclude that the net change in the equivalent inductor voltage $v_L$ is zero over one electric cycle, i.e.,

$$\int_{t}^{t+T_s} v_L dt = DT_s\left[2V_{\rm emf} - i_a(2R)\right] + D'T_s\left[2V_{\rm emf} - i_a(2R) - V_{\rm dc}\right] = 0 \quad (1)$$

$$i_a = 2 \cdot \frac{V_{\rm emf}}{D'^2 \cdot R_b + 2R} \quad (2)$$

where $T_s$ is the switching period, $V_{\rm emf}$ is the back EMF, and $i_a$ is the armature current. Similarly, according to the principle of the capacitor charge balance, one will have

$$\int_{t}^{t+T_s} i_{\rm dc} dt = DT_s\left(-\frac{V_{\rm dc}}{R_b}\right) + D'T_s\left(i_a - \frac{V_{\rm dc}}{R_b}\right) \quad (3)$$

where $D$ is the duty cycle satisfying $D + D' = 1$. Substituting (2) into (3), the charging voltage $V_{\rm dc}$ can be described in terms of $D'$, the internal resistance $R$ of the armature, and the equivalent load resistance $R_B$, i.e.,

$$T(D') = \frac{V_{\rm dc}}{V_{\rm emf}} = 2 \cdot \frac{1}{D' + 2\frac{K}{D'}} \quad (4)$$

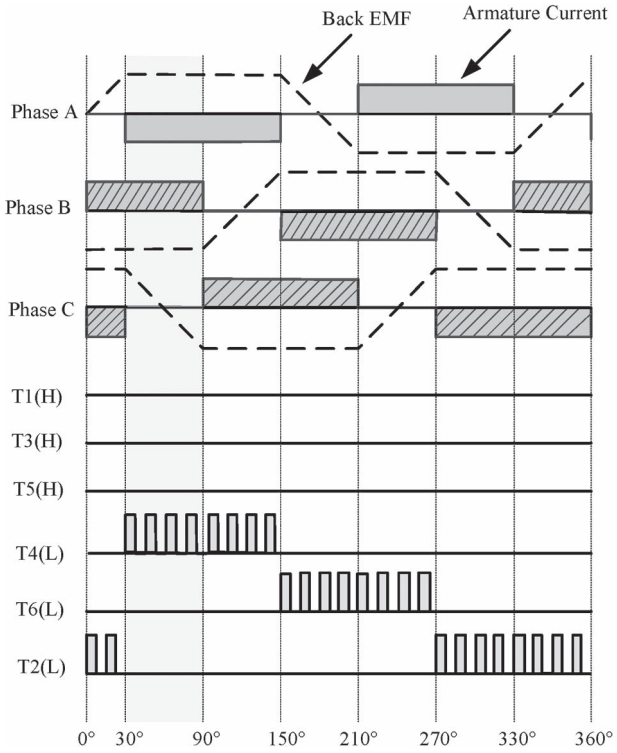


Fig. 5. Regenerative braking with single switch.

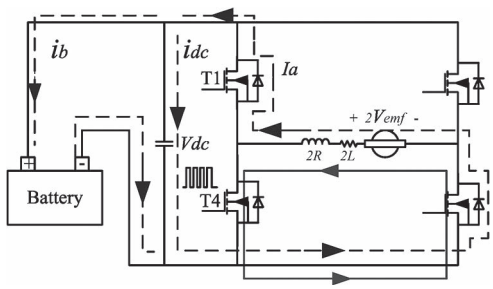


Fig. 6. Equivalent circuit of the single switch.

where $K$ is defined as $R/R_b$.

To evaluate the maximum conversion ratio of the switching strategy, we differentiate (4) with respect to $D'$ to obtain

$$\frac{dT}{dD'} = 2 \cdot \frac{(2K - D'^2)}{(D'^2 + 2K)^2}. \tag{5}$$

By letting (5) be equal to 0, we can obtain the value of $D'$ which maximizes (4) as follows:

$$T_{\max}(D')|_{D'=\sqrt{2K}} = 2 \cdot \frac{1}{2\sqrt{2K}} = \frac{1}{\sqrt{2K}} \tag{6}$$

when $K$ increases from 0 to 1. It should be noted that the maximum conversion ratio is smaller than 1 for the case where $K > 0.5$. In other words, the output voltage of the alternator commutation will be smaller than the back EMF, i.e., the dynamic energy of the EVs will be transferred into braking torque and heat instead of being recovered into the battery. Fig. 7 shows the relation.

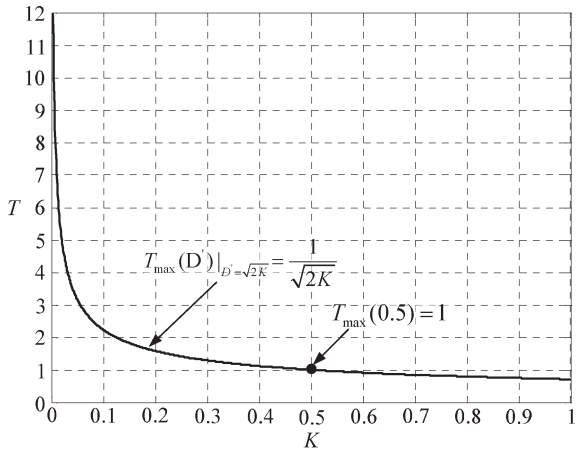


Fig. 7. Maximum conversion ratio versus $K$ for regenerative braking with single switch.

## III. EV Modeling

The modeling of the EV has been done in MATLAB/Simulink. The driver block makes a torque request which propagates through various powertrain system component and realizes vehicle motion. System-level simulators have been modeled by using empirical data that are based on measurements supplied by component manufacturers or extended from measurements obtained from literature sources. These are modeled in Simulink as look-up tables. Other component models are physical or analytical in nature and are modeled by mathematical equations [18].

The EV model weighs about 1325 kg inclusive of battery. The vehicle has a frontal area of 2.57 $m^2$, with a drag coefficient of 0.3 and rolling resistance of 0.00268 Ω. The values assigned are based on a rough estimate of a mid-sized car. The electric motor chosen is a BLDC motor with a peak power of 40 kW. The battery pack is a Li-Ion battery. It has a nominal voltage of 72 V, with energy content of 1.2 kWh and weight around 20 kg.

### A. Driver Subsystem

The driver block delivers the desired drive torque and the desired brake torque through the activation of the accelerator and brake pedal, respectively. If the driver wishes to accelerate the vehicle, he depresses the accelerator. Depending on the amount of depression of the accelerator pedal, a corresponding driver torque request is sent to the vehicle through various powertrain systems such as the battery and motor models. The regeneration starts only when the brake pedal is pressed. Once the brake pedal is depressed, in accordance with the position of the brake pedal, a corresponding proportion of brake torque is applied. Then, the brake torque due to the regenerative brake control strategy is divided into regenerative braking and friction braking [6]. The amount of mechanical energy consumed by a vehicle when driving a prespecified driving pattern mainly depends on three factors: the aerodynamic friction losses, the rolling friction losses, and the energy dissipated in the brakes. The elementary equation that describes the longitudinal dynamics of a road vehicle has the following form:

$$m_v \frac{dv(t)}{dt} = F_t(t) - F_a(t) - F_r(t) - F_g(t) \tag{7}$$

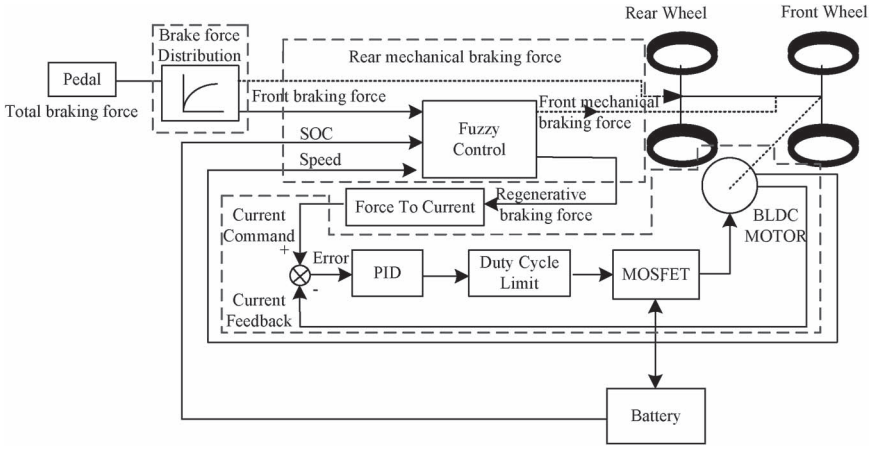


Fig. 8. Structure of the control strategy system.

where $m_v$ is the vehicle mass (in kilograms), $v$ is the vehicle speed (in meters per square second), $F_a$ is the aerodynamic friction (in newtons), $F_r$ is the rolling friction (in newtons), and $F_g$ is the force caused by gravity when driving on nonhorizontal roads (in newtons).

The traction force $F_t$ is the force generated by the prime mover minus the force which is used to accelerate the rotating parts inside the vehicle and then minus all friction losses in the powertrain.

*1) Aerodynamic Friction Losses:* Usually, the aerodynamic resistance force $F_a$ is approximated by simplifying the vehicle to be a prismatic body with a frontal area $A_f$. The force caused by the stagnation pressure is multiplied by an aerodynamic drag coefficient $C_d$ to model the actual flow conditions

$$F_a(v) = \frac{1}{2}\rho_a A_f C_d v^2. \tag{8}$$

Here, $v$ is the vehicle speed (in meters per square second), and $\rho_a$ is the density of ambient air (in kilograms per cubic meter). The parameter $C_d$ is the coefficient of drag estimated using computational fluid dynamics programs or experiments in wind tunnels. To estimate the mechanical energy, it is required to drive a typical test cycle, and this parameter may be assumed to be constant.

*2) Rolling Friction Losses:* The rolling friction is modeled as

$$F_r = C_r m_v g \cos(\alpha) \tag{9}$$

where $m_v$ is the vehicle mass (in kilograms), $g$ is the acceleration due to gravity (in meters per square second), $C_r$ is the rolling friction coefficient, and $\alpha$ is the slope angle (in degrees). The rolling friction coefficient $C_r$ depends on many variables. The most important influencing quantities are vehicle speed $v$, tire pressure $p$, and road surface conditions. For many applications, particularly when the vehicle speed remains moderate, the rolling friction coefficient $C_r$ may be assumed to be constant.

*3) Uphill Driving Force:* The force induced by gravity when driving on a nonhorizontal road is conservative and considerably influences the vehicle behavior. In this paper, this force will be modeled by

$$F_g = m_v g \sin(\alpha). \tag{10}$$

### *B. EM*

The power from the battery drives the electric machine (EM). The EM works as a motor to propel the vehicle when positive power is fed in and as a generator when negative power is fed in. EM is modeled as a look-up table with motor-generator characteristics (efficiency curve) of a BLDC motor MC_PM8 of 8 kW from ADVISOR. This motor is downsized to that of 8 kW to meet the specifications provided. Downsizing is done by reducing the torque with a scale factor determined by the ratio of the default power (8 kW) and the required power (7 kW).

### *C. Brake Strategy Subsystem*

The structure of the control strategy system is shown in Fig. 8. Through the pedal sensor, we can obtain the driver's required braking force. According to the distribution regulations of braking force among front and rear wheels, the front braking force and the rear braking force can be calculated, respectively. According to the fuzzy logic controller, we can obtain the value of the regenerative braking force. Then, the front mechanical braking force, the regenerative braking force, and the rear braking force can be attained [8], [9].

At last, the regenerative braking force is translated into braking current through

$$I_{\rm com} = k_1 F_{\rm reg} \tag{11}$$

i.e., the braking current $I_{\rm com}$ is proportional to the regenerative braking force $F_{\rm reg}$, and $k_1$ is the scale factor [10].

*1) Distribution of the Braking Force:* In RBS of EVs, the braking force is mainly the wheel braking force $F_{\rm front}$ and rear-wheel braking force $F_{\rm rear}$. For the front-wheel drive EVs, the front-wheel braking force is composed of two parts: front-wheel frictional braking force and regenerative braking force. Therefore, brake force distribution refers to total braking force $\Sigma F$ in the allocation of front and rear wheels, rear-wheel friction, and regenerative braking force distribution and coordination issues. A braking force distribution of the front and rear wheels of the EVs in the ideal case is given by [3], [11]

$$F_{\rm rear}=\frac{1}{2}\left[\frac{mg}{h_g}\sqrt{b^2+\frac{4h_gL}{mg}F_{\rm front}}-\left(\frac{mgb}{h_g}+2F_{\rm front}\right)\right]. \tag{12}$$

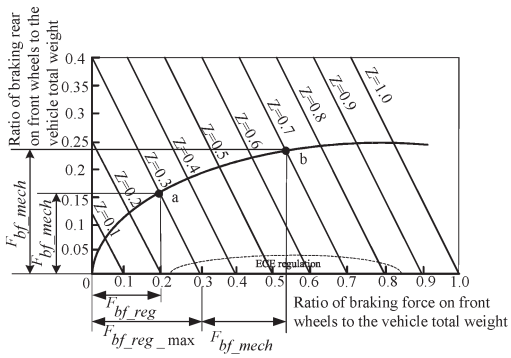


Fig. 9. EV front and rear force distribution.

In (12), $m$ is the quality of the EV, $b$ is the centroid of the EV to the rear axle centerline distance (in meters), $h_g$ is the height of the centroid of the EV, and $L$ is the distance between the front and rear axles of the EV (in meters). In Fig. 9, $z$ is the braking strength, which is defined as $z = d_v/d_t/g$, where $v$ is the EVs' speed and $g$ is the acceleration of gravity. The front- and rear-wheel braking force allocation strategy of the EVs is as follows: When $z < 0.1$, the total braking force $\Sigma F$ is all borne by the drive wheel, and the front wheel is not involved in the braking of the vehicle. When $0.1 < z < 0.7$, the braking force is allocated by electromechanical composite brake. According to (12), it can be learned that, when the EV front and rear wheels are locked, the ideal braking force distribution curve ($I$ curve) is shown in Fig. 9 [3]. Given in any adhesion coefficient of the road with the front and rear wheels simultaneously locking of the conditions are the following: The front- and rear-wheel braking forces are equal to adhesion $\phi$, and there holds

$$\begin{cases} F_{\text{front}} + F_{\text{rear}} = \phi mg \\ \dfrac{F_{\text{front}}}{F_{\text{rear}}} = \dfrac{b + \phi h_g}{a + \phi h_g}. \end{cases} \tag{13}$$

In (13), $\phi$ is the adhesion coefficient of the road and wheels. $a$ is the distance (in meters) from the centroid to the front axle centerline. Through the pedal sensor, we can obtain the driver required braking force [3], [11].

*2) Fuzzy Control:* Braking force distribution in EVs with regeneration is influenced by many factors, and many parameters are constantly changing, so recycling strategy is difficult to be expressed. The fuzzy logic control strategy for EV braking force distribution can be easily demonstrated by the influence of different factors. Therefore, the fuzzy control theory is applied to the EV braking force distribution. The fuzzy control strategy of the EV braking force distribution structure is shown in Fig. 8; the three inputs are the EV front-wheel braking force, speed, and battery charge state [state of charge (SOC)] [12].

In the fuzzy control system, the input variables include the front braking force, the SOC, and the EV speed. The output variable is the ratio which is proportional to the regenerative braking force taking in the front braking force. *Front braking force*: the driver braking requirements are concerned with the driving safety. The value of the braking force represents the braking distance and time the driver requires. We prefer the concourse of speed to be low, middle, and high, and the universe of discourse is [0, 2000]. The membership functions are

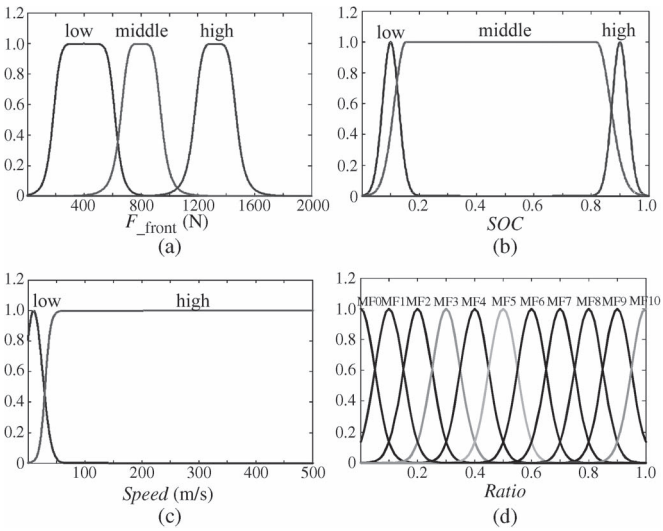


Fig. 10. Membership functions of fuzzy control. (a) Membership function of the front braking force. (b) Membership function of the SOC. (c) Membership function of speed. (d) Membership function of ratio.

shown in Fig. 10(a). *SOC*: when the battery's SOC is less than 10%, the internal resistance of the battery is high, unsuitable charging in this case; the regenerative braking force should be a smaller proportion. When the SOC is between 10% and 90%, the battery can be charging with a large current; the ratio of the regenerative braking force should be correspondingly increased. When the SOC is greater than 90%, the charging current should be reduced to prevent the excessive charging of the battery; the value of the regenerative braking force should be lower. We prefer the set of SOC to be low, middle, and high, and the universe of discourse is [0, 1]. The membership functions are shown in Fig. 10(b) [13]. *Speed*: vehicle speed plays an important role in ensuring the brake safety. To ensure the brake safety and to comply with the relevant legislation, the regenerative braking force should be a low proportion when the speed is low. The regenerative braking force can be increased to an appropriate level when the speed is intermediate. When speed is high, we can increase the ratio of the regenerative braking force to the biggest value. We prefer the set of speed to be low and high, and the universe of discourse is [0, 500]. The membership functions can be seen in Fig. 10(c). *Output variables*: the type of the fuzzy logic controller is Mamdani. Ratio $= \{MF0, MF1, MF2, MF3, MF4, MF5, MF6, MF7, MF8, MF9, MF10\} = (0, 0.1, 0.2, 0.3, 0.4, 0.5, 0.6, 0.7, 0.8, 0.9, 1.0)$. The membership functions can be seen in Fig. 10(d).

Fuzzy control rules: the front braking force is L, M, and H; SOC is L, M, and H; and speed is L and H. We prefer the rules shown in Table I.

*3) Proportional–Integral–Derivative (PID) Control:* With PID control used primarily to ensure a constant brake torque, different braking force values will give different PWMs. It is supposed that PID control can quickly adjust the desired PWM in order to maintain braking torque constantly. A constant electrical braking torque can be achieved during the fuzzy inference. When the fuzzy reasoning is slower than PID control, the braking torque can be real-time controlled by PID control [14].

TABLE I
FUZZY LOGIC CONTROL RULES

| Speed | SOC | $F_{front}$ | MF | Speed | SOC | $F_{front}$ | MF |
|---|---|---|---|---|---|---|---|
| L | L | L | 2 | H | L | L | 5 |
| L | L | M | 1 | H | M | M | 5 |
| L | L | H | 0 | H | H | H | 4 |
| L | M | L | 4 | H | L | L | 10 |
| L | M | M | 2 | H | M | M | 9 |
| L | M | H | 3 | H | H | H | 8 |
| L | H | L | 3 | H | L | L | 5 |
| L | H | M | 1 | H | H | M | 3 |
| L | H | H | 2 | H | M | H | 1 |

### *D. Battery Subsystem*

The power request from the driver block after translating through the brake control strategy subsystem reaches the battery subsystem. Here, the positive power discharges the battery, and the negative power charges the battery. The battery is modeled as a look-up table with the battery characteristics of a lithium-ion (ESS_Li7) battery from ADVISOR 3.0. rapidly assessing the performance and fuel economy of conventional, electric, hybrid, and fuel cell vehicles. The user can obtain datasheets, make changes to vehicle and component specifications, and run them on various test conditions. The battery is set with an initial SOC of 90%. When the positive power is fed in, it enables the discharge block. In the discharge block depending on the SOC level, we obtain the maximum module voltage that can be supplied, from the plot of SOC versus voltage of the battery module. This module voltage is then multiplied with a number of cells in series to obtain the battery pack voltage. Then, from the power demand and the maximum possible voltage at that SOC, we calculate the current that can be supplied to the motor. This current is limited by the maximum amount of current that the motor can handle. When a negative power is fed in, the charge block becomes enabled. In the charge block depending on the SOC level and as explained previously, we calculate the maximum possible battery voltage and current that can be fed into the battery. This current is again limited by the maximum current capability of the generator. When the power request is zero, i.e., the vehicle comes to rest or when the braking power is too low to generate a significant current, the battery idle block is enabled. No current is withdrawn or put back during this phase.

### *E. Vehicle Subsystem*

The electromechanical torque produced by the motor is fed into the vehicle subsystem to propel the vehicle. The vehicle model used is the TNO Delft tyre sim mechanics vehicle model. This model has a central body subsystem and four tire subsystems. The tire subsystems are designed based on Prof. Pacekja's famous magic formula for describing tires. Tires have a dimension of 205/60 R15. The road surface is dry asphalt, and the coefficient of friction offered by the surface is 1. The Delft tyre model helped in keeping a watch on the variation of longitudinal slip, hence making sure that, at no point during the simulation, wheel lock can occur. A wheel lock is undesirable because it would prevent regeneration and destabilize the vehicle.

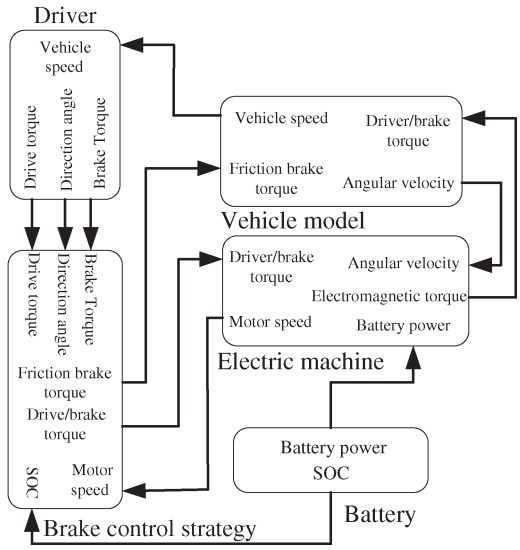


Fig. 11. Braking force distribution.

## IV. OPTIMAL BRAKING PERFORMANCE AND RBS EFFICIENCY

In recent years, more and more advanced braking systems are in development, which allow us to control the braking force on each wheel independently. The fully controllable hybrid brake system can be controlled to apply braking forces on the front and rear wheels by following the ideal braking force distribution curve (Fig. 11). This control strategy can obtain optimal brake performance. Fig. 9 illustrates the principle of this control strategy for the vehicle on which electric regenerative braking is available only on front wheels. When the required total braking force on the front wheels is smaller than that produced by the electric motor, the electric motor produces the total braking force, and no mechanical braking force is applied. Nevertheless, the mechanical braking produces the total braking force for the rear wheels to follow the $I$-curve, as shown by point a in Fig. 9. When the required total braking force on the front wheels is greater than that produced by the electric motor, both electric and mechanical brakes have to be applied. For more braking energy recapture, the electric motor should be controlled to produce its maximum braking force that is limited by the electric motor or energy storage. As shown by point b in Fig. 9, the remaining is applied by the mechanical brake. It should be noted that, in low front-wheel speed caused by the actual low vehicle speed or closely locked wheels, it is hard for the electric motor to produce the braking torque due to the low electric motive force (voltage) generated in the stator windings of the electric motor. Therefore, in this case, the mechanical brake has to produce the total braking force as required. As seen in Fig. 9, a significant amount of braking energy is consumed by the rear brake, especially for weak braking (small deceleration). For example, at $z = 0.3$, around 33% of the total braking energy is consumed by the rear brake; at $z = 0.1$, this percentage reaches

37.8%. The battery should take into account the relationship between the SOC and its charging characteristics. In this paper, the input/output power and SOC of the battery are calculated using the internal resistance model of the battery. The internal resistance is obtained through experiments on the SOC of the battery. The following equations describe the battery's SOC at discharge and charge. At discharge

$$\mathrm{SOC}_{\mathrm{dis}} = \mathrm{SOC} - Q_m^{-1} \int_{t_i}^{t_i+T_s} \eta_A(i_{a,\tau})^{-1} i_a(t) dt \tag{14}$$

at charge

$$\mathrm{SOC}_{\mathrm{chg}} = \mathrm{SOC} + Q_m^{-1} \int_{t_i}^{t_i+T_s} i_a(t) dt \tag{15}$$

where $\mathrm{SOC}_{\mathrm{dis}}$ is the electric discharge quantity at discharge mode, $\mathrm{SOC}_{\mathrm{chg}}$ is the charge quantity of the battery, $Q_m$ is the battery capacity, and $\eta_A(i_a, \tau)$ is the battery efficiency. In the braking process on a flat road, the vehicle's kinetic energy and regenerative electrical energy are calculated by the following:

$$\epsilon = \frac{\sum E_{\mathrm{bat}}}{\sum E_{\mathrm{kin}}} \tag{16}$$

with kinetic energy

$$E_{\mathrm{kin}} = \sum \frac{1}{2} m \left(V_2^2 - V_1^2\right) \tag{17}$$

and electrical energy

$$E_{\mathrm{bat}} = \int_{t=0}^{t=\mathrm{end}} (E_k = I_t R_t I_i) dt \tag{18}$$

where $E_k$ is the battery voltage, $I(t)$ is the battery current, $R(t)$ is the charging resistance, $V_1$ is the initial velocity, and $V_2$ is the final velocity.

## V. Simulation Results

Under the environment of MATLAB and Simulink, the RBS is modeled, and the drive cycle is performed. The test is performed according to urban driving schedules. The simulation results and test are represented as follows.

### A. Dynamic Performance and Force Distribution at Different Brake Pedal Inputs

At different braking scenarios, we simulated the dynamic performance of the car and force distribution due to different brake pedal inputs. The simulation is run for a period of 50 s. The car reaches a maximum velocity of 20 m/s, and then, it starts braking. Regenerative braking is only in the front because the car is front driven. In one case, a small brake pedal input is applied. The deceleration achieved is very small, depicting a congested city traffic scenario. In Fig. 12, it is evident from the plots that, when the brake pedal is depressed, the vehicle starts

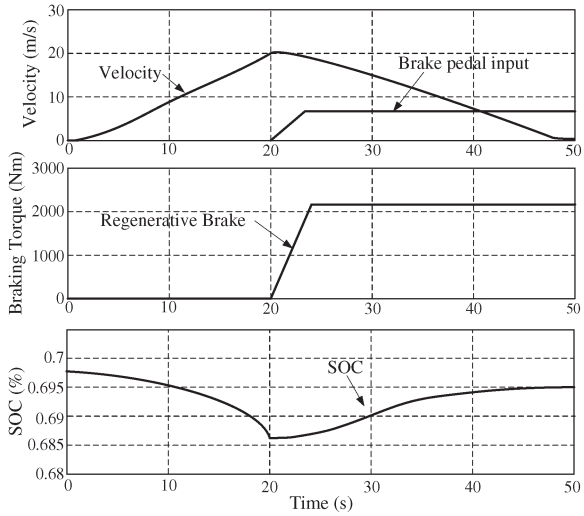


Fig. 12. Simulation EV speed curve.

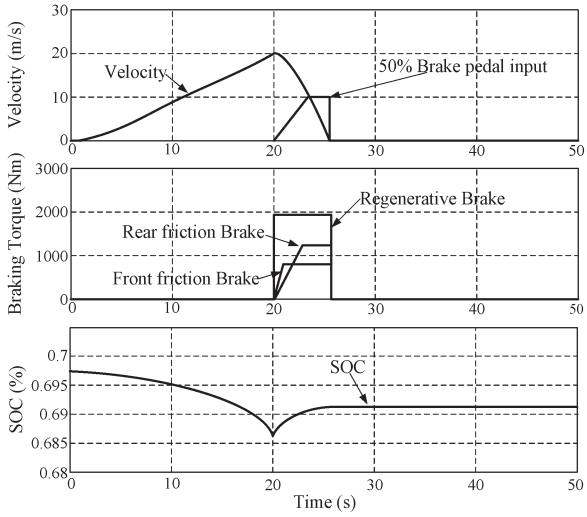


Fig. 13. Simulation EV speed curve.

decelerating at a small rate. The brake torque corresponding to this brake pedal input is small, so that the entire braking torque could be provided by the generator. Hence, we observe in the second subplot that the braking is just purely regenerative, and hence, an appreciable SOC increment is observed in the third subplot.

Figs. 13 and 14 show the simulation results of 50% brake pedal depressed and full brake pedal depressed, respectively. The following equations are used to calculate the amount of brake torque required to stop the vehicle in the stopping distance prescribed by the drive cycle. In the MATLAB/Simulink model, the motor parameters are as follows: power $P_e = 40$ kw, maximum current $I_{\max} = 600$ A, minimum voltage $V_{\min} = 60$ v, maximum motor torque $T_m = 520.88$ NM, and maximum regenerative torque $T_{\mathrm{reg}} = 322.7$ NM. The vehicle characteristics are as follows: mass of the vehicle $M_v = 1325$ kg, frontal area $A_f = 2.57$ m$^2$, drag coefficient $C_w = 0.30$, air density $\rho = 1.2$ kg/m$^3$, radius of the wheel $R_w = 0.3$ m, and rolling resistance coefficient $C_{\mathrm{roll}} = 0.008$. Required brake force

$$F_x = M_v a + \frac{1}{2} \rho C_w A_f V^2 + C_{\mathrm{roll}} mg \tag{19}$$

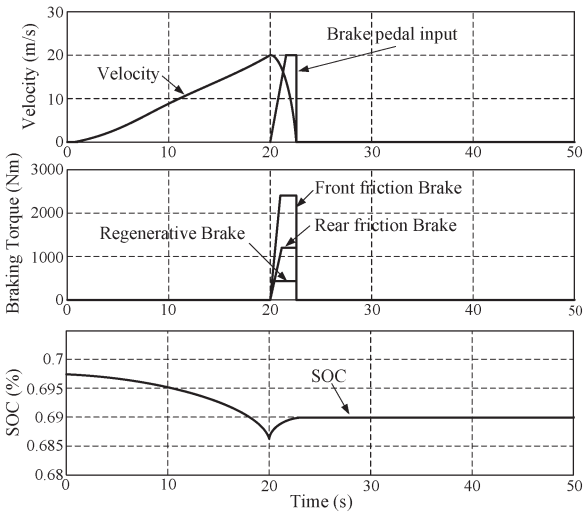


Fig. 14. Simulation EV speed curve.

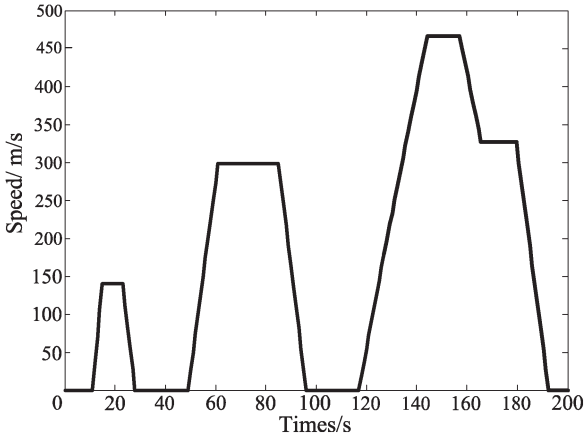


Fig. 15. Simulation EV speed curve.

so we can obtain the equation

$$F_x = 1325a + 0.4009v^2 + 104. \tag{20}$$

Through this way, we can calculate the amount of brake torque required to stop the vehicle in the stopping distance prescribed by the drive cycle. For example, if we have to stop the car at a speed of 25 m/s$^2$, with $a = -3$ m/s$^2$, the brake force is

$$F_x = 1325 \times (-3) + 0.4009 \times 25^2 + 104 = -3620.43 \text{ N}. \tag{21}$$

At the same time, the amount of brake torque is

$$T_b = F_x R_w = -3602.43 \times 0.3 = 1080.7 \text{ N} \cdot \text{m}. \tag{22}$$

### B. Simulation EV Speed Curve

As shown in Fig. 15, it is composed of three stages of accelerating, four stages of running at constant speed, four stages of decelerating, and two idle stages, which is specified in the standard of GT/T18386-2005 [15].

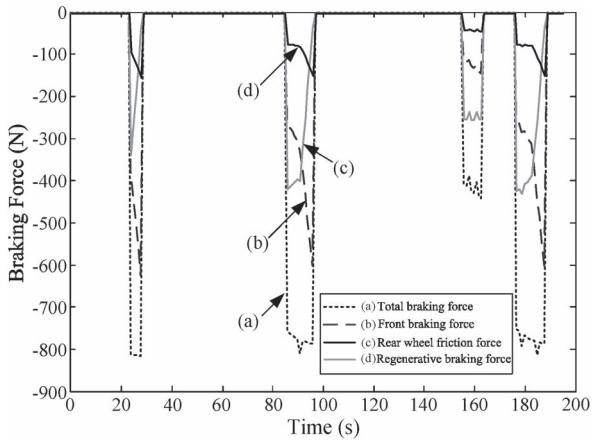


Fig. 16. Braking force distribution.

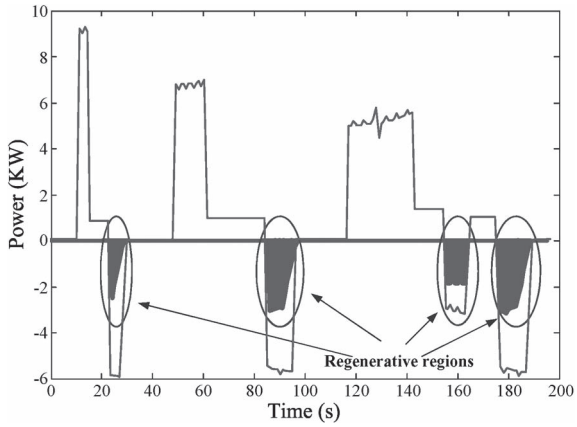


Fig. 17. Energy regeneration when braking.

### C. Results of Braking Force Distribution

Fig. 16 shows the distribution of the braking force. The (a) curve represents the total required braking force; the (b) curve, (c) curve, and (d) curve represent the rear-wheel friction braking force, front braking force, and regenerative braking force, respectively. From Fig. 16, we can conclude that the friction braking force of the front wheel is smaller than the regenerative braking force, and the front-wheel braking force is provided mainly by the electrical braking in deceleration time of the EV. The higher the speed is, the greater the proportion of electrical brake is, which proves that high speed is more suitable for the regenerative braking.

### D. Energy Recovery Efficiency

In a whole urban driving cycle, there are four stages of decelerating in which the battery can partly recover the EV kinetic energy. As shown in Fig. 17, the shadow part is the recover energy whose ratio is about 50%. However, the ratio is related to the EV speed, traffic information, SOC, and driver's habits closely.

### E. Current Curve of the BLDC Motor DC Bus

As shown in Fig. 18, the current in the BLDC motor dc bus is related to the speed. When the EV brakes, the RBS can control the current of the BLDC motor to ensure the constant torque by

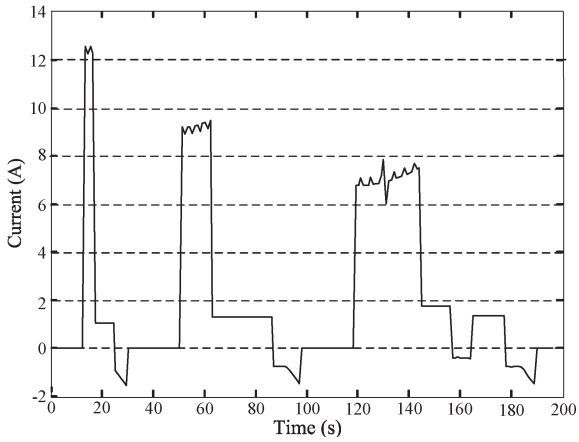


Fig. 18. Current curve on the BLDC motor dc bus with PID control.

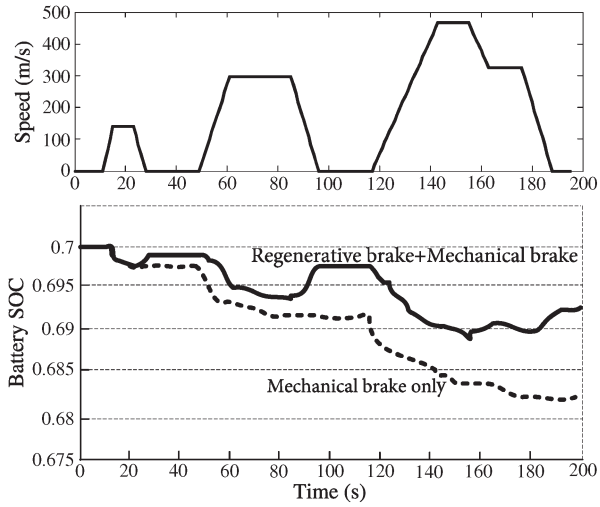


Fig. 19. Battery's SOC change.

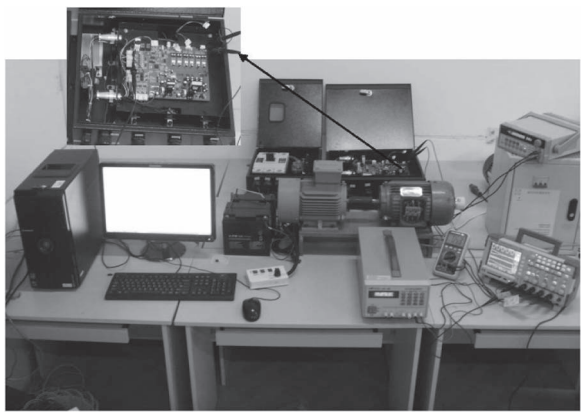

Fig. 20. Practical implementation.

the PID controller. The PID controller adjusts the ratio of PWM to realize the BLDC motor control.

### *F. Battery SOC Change*

The battery SOC can demonstrate EV energy consumption intuitively. As shown in Fig. 19, in a whole urban driving cycle, the EV acceleration process consumes more energy than the other processes, and the corresponding battery SOC declines faster. In stages of decelerating, the SOC curve rises slightly, which demonstrates that regenerative braking is working.

TABLE II
MOTOR SPECIFICATIONS

| *Description* | *value* |
|---|---|
| Rated Voltage | 72 V |
| Rated Current | 200 A |
| Rated Speed | 2800 rpm |
| Rated Power | 7 KW |
| Number of Poles | 8 |

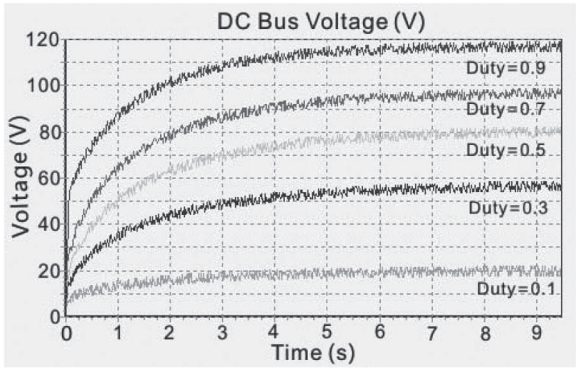


Fig. 21. DC bus voltage of different duties but at the same speed.

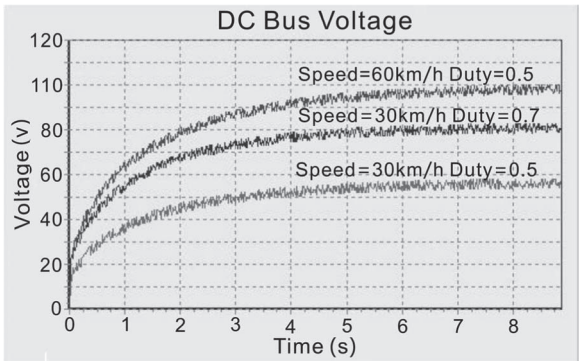


Fig. 22. DC bus voltage at the same speed.

## VI. APPLICATION

The RBS described previously has been successfully type tested. In the real test system shown in Fig. 20, we use the TMS320F2812 as the control chip, and the specifications of the motor are listed in Table II.

As shown in Fig. 21, we can obtain different voltages for different PWM duties with the same speed. Therefore, at different speeds, we can adjust the PWM duty to obtain different voltages. In Fig. 21, we made the speed 60 km/h. Through adjusting the PWM duty, the dc bus voltage can reach and is even over the rated voltage. At the same time, when the speed is 30 km/h, 50% of the PWM duty can make the dc bus voltage reach the rated voltage, so we can adjust the PWM duty to 70% and the voltage rise as shown in Fig. 22.

Fig. 23 shows the voltage, current, and speed waveforms at the breaking state. When the EV speed descends from 70 km/h

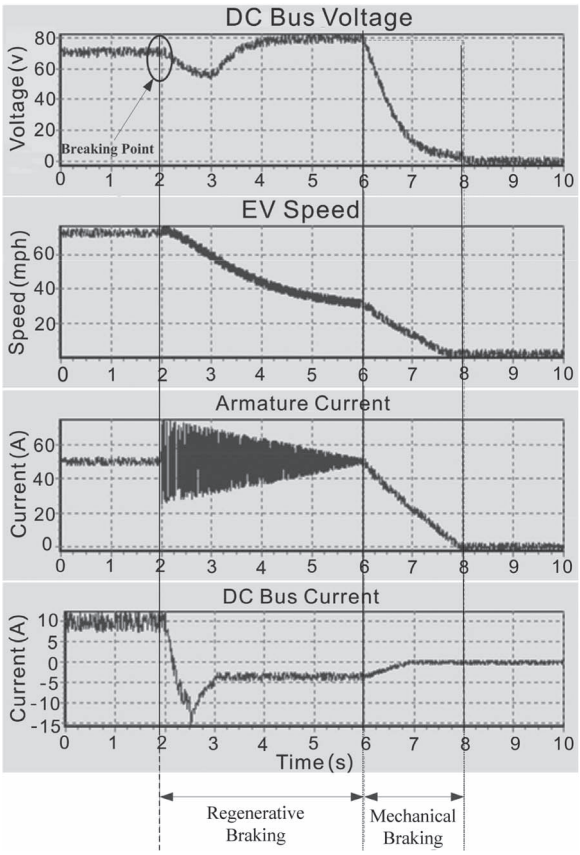


Fig. 23. Voltage, current, and speed waveforms at the breaking state.

to about 30 km/h, the dc bus voltage keeps a high value at the regenerative region. The EV will switch to mechanical braking if the speed is too low. At the same time, the dc current will descend to 0 when EV stops.

## VII. Conclusion

This paper has presented the RBS of EVs which are driven by the BLDC motor. The performance of the EVs' regenerative brake system has been realized by our control scheme which has been implemented both in the simulation and in the experiments. By combining fuzzy control and PID control methods which are both sophisticated methods, RBS can distribute the mechanical braking force and electrical braking force dynamically. PID control is a very popular method in electric car control, but it is difficult to obtain a precise brake current. Braking force is affected by many influences such as SOC, speed, brake strength, and so on. In this paper, we have chosen the three most important factors: SOC, speed, and brake strength as the fuzzy control input variables. We have found that RBS can obtain appropriate brake current, which is used to produce brake torque. At the same time, we have adopted PID control to adjust the BLDC motor PWM duty to obtain the constant brake torque. PID control is faster than fuzzy control, so the two methods combined together can realize the smooth transitions. Similar results are obtained from the experimental studies. Therefore, it can be concluded that this RBS has the ability to recover energy and ensure the safety of braking in different situations.

## References

[1] P. J. Grbovic, P. Delarue, P. Le Moigne, and P. Bartholomeus, "A bidirectional three-level dc-dc converter for the ultra-capacitor applications," *IEEE Trans. Ind. Electron.*, vol. 57, no. 10, pp. 3415–3430, Oct. 2010.

[2] F. Wang, X. Yin, H. Luo, and Y. Huang, "A series regenerative braking control strategy based on hybrid-power," in *Proc. Int. Conf. CDCIEM*, 2012, pp. 65–69.

[3] N. Mutoh and Y. Nakano, "Dynamics of front-and-rear-wheel-independent-drive-type electric vehicles at the time of failure," *IEEE Trans. Ind. Electron.*, vol. 59, no. 3, pp. 1488–1499, Mar. 2012.

[4] M. Cheng, W. Hua, J. Zhang, and W. Zhao, "Overview of stator-permanent magnet brushless machines," *IEEE Trans. Ind. Electron.*, vol. 58, no. 11, pp. 5087–5101, Nov. 2011.

[5] Y. Wang and Z. Deng, "Hybrid excitation topologies and control strategies of stator permanent magnet machines for dc power system," *IEEE Trans. Ind. Electron.*, vol. 59, no. 12, pp. 4601–4616, Dec. 2012.

[6] C. Sheeba Joice, S. R. Paranjothi, and V. J. Senthil Kumar, "Digital control strategy for four quadrant operation of three phase BLDC motor with load variations," *IEEE Trans. Ind. Informat.*, vol. 9, no. 2, pp. 974–982, May 2013.

[7] A. Sathyan, N. Milivojevic, Y.-J. Lee, M. Krishnamurthy, and A. Emadi, "An FPGA-based novel digital PWM control scheme for BLDC motor drives," *IEEE Trans. Ind. Electron.*, vol. 56, no. 8, pp. 3040–3049, Aug. 2009.

[8] N. Keskar, M. Batello, A. Guerra, and A. Gorgerino, "Power Loss Estimation in BLDC Motor Drives Using iCalc," International Rectifier, El Segundo, CA, USA, Rep. AN-1048, Feb. 2010.

[9] K. Yoong, Y. H. Gan, G. D. Gan, C. K. Leong, Z. Y. Phuan, B. K. Cheah, and K. W. Chew, "Studies of regenerative braking in electric vehicle," in *Proc. IEEE Conf. Sustainable Utilization Develop. Eng. Technol.*, Nov. 20/21, 2010, pp. 40–41.

[10] J. M. J. Yang, H. L. Jhou, B. Y. Ma, and K. K. Shyu, "A cost-effective method of electric brake with energy regeneration for electric vehicles," *IEEE Trans. Ind. Electron.*, vol. 56, no. 6, pp. 2203–2212, Jun. 2009.

[11] N. Mutoh, "Driving and braking torque distribution methods for front- and rear-wheel-independent drive-type electric vehicles on roads with low friction coefficient," *IEEE Trans. Ind. Electron.*, vol. 59, no. 10, pp. 3919–3933, Oct. 2012.

[12] C.-H. Huang, W.-J. Wang, and C.-H. Chiu, "Design and implementation of fuzzy control on a two-wheel inverted pendulum," *IEEE Trans. Ind. Electron.*, vol. 58, no. 7, pp. 2988–3001, Jul. 2011.

[13] P. J. Grbovic, P. Delarue, P. Le Moigne, and P. Bartholomeus, "The ultracapacitor based controlled electric drives with braking and ride-through capability: Overview and analysis," *IEEE Trans. Ind. Electron.*, vol. 58, no. 3, pp. 925–936, Mar. 2011.

[14] K. Ang, G. Chong, and Y. Li, "PID control system analysis, design and technology," *IEEE Trans. Control Syst. Technol.*, vol. 13, no. 3, pp. 559–576, Jul. 2005.

[15] *The National Standards of PR China GB/T 18386-2005, Electric Vehicles Energy Consumption and Range-Test Proceeding*, China Standards Press, Beijing, China, 2005.

[16] E. Bostanci, Z. Neuschl, and R. Plikat, "No-load performance analysis of brushless dc machines with axially displaceable rotor," *IEEE Trans. Ind. Electron.*, vol. 61, no. 4, pp. 1692–1699, Apr. 2014.

[17] Y.-T. Chen, C.-L. Chiu, Y.-R. Jhang, and Z.-H. Tang, "A driver for the single-phase brushless dc fan motor with hybrid winding structure," *IEEE Trans. Ind. Electron.*, vol. 60, no. 10, pp. 4369–4375, Oct. 2013.

[18] A. Dadashnialehi, A. Bab-Hadiashar, Z. Cao, and A. Kapoor, "Intelligent sensorless ABS for in-wheel electric vehicles," *IEEE Trans. Ind. Electron.*, vol. 61, no. 4, pp. 1957–1969, Apr. 2014.

**Xiaohong Nian** received the B.S. degree from Northwest Normal University, Lanzhou, China, in 1985, the M.S. degree from Shandong University, Jinan, China, in 1992, and the Ph.D. degree from Peking University, Beijing, China, in 2004.

He is a Professor with Central South University, Changsha, China. His research interests cover theory of decentralized control for networked control of multiagent systems, induction motor control, and converter technology and motor drive control.

**Fei Peng** received the M.S. degree in control science and engineering from the School of Information Science Engineering, Central South University, Changsha, China, in 2013.

He is currently an Engineer with Guangzhou Automobile Group Company, Ltd., Automotive Engineering Institute, Guangzhou, China. His current research interests include automotive electronics and clean energy, traction control/antilock breaking and control of active magnetic bearings for high-speed machines, sensorless control of brushless machines, and analysis and design of resonant converter systems.

**Hang Zhang** received the B.S. degree in automation from Nanjing University of Chemical Technology (now Nanjing University of Technology), Nanjing, China, in 1988 and the M.S. degree and the Ph.D. degree in information engineering and control from the School of Information Science and Engineering, Central South University, Changsha, China, in 2002 and 2006, respectively.

His current research interests include image processing and advanced controls and their applications in intelligent transportation systems and industry.